

Zero Dynamics, Pendulum Models, and Angular Momentum in Feedback Control of Bipedal Locomotion

Yukai Gong and Jessy Grizzle

Abstract—Low-dimensional models are ubiquitous in the bipedal robotics literature. On the one hand is the community of researchers that bases feedback control design on pendulum models selected to capture the center of mass dynamics of the robot during walking. On the other hand is the community that bases feedback control design on virtual constraints, which induce an exact low-dimensional model in the closed-loop system. In the first case, the low-dimensional model is valued for its physical insight and analytical tractability. In the second case, the low-dimensional model is integral to a rigorous analysis of the stability of walking gaits in the full-dimensional model of the robot. *This paper seeks to clarify the commonalities and differences in the two perspectives for using low-dimensional models. In the process of doing so, we argue that angular momentum about the contact point is a better indicator of robot state than linear velocity. Concretely, we show that an approximate (pendulum and zero dynamics) model parameterized by angular momentum provides better predictions for foot placement on a physical robot (e.g., legs with mass) than does a related approximate model parameterized in terms of linear velocity. We implement an associated angular-momentum-based controller on Cassie, a 3D robot, and demonstrate high agility and robustness in experiments.*

Index Terms—Bipedal robots, zero dynamics, pendulum models, angular momentum

I. INTRODUCTION

Models of realistic bipedal robots tend to be high-dimensional, hybrid, nonlinear systems. This paper is concerned with two major themes in the literature for “getting around” the analytical and computational obstructions posed by realistic models of bipeds.

On the one hand are the broadly used, simplified pendulum models [1]–[7] that provide a computationally attractive model for the center of mass dynamics of a robot. When used for control design, the fact that they ignore the remaining dynamics of the robot generally makes it impossible to prove stability properties of the closed-loop system. Despite the lack of analytical backing, the resulting controllers often work in practice when the center of mass is well regulated to match the assumptions underlying the model. Within this context, the dominant low-dimensional pendulum model by far is the so-called linear inverted pendulum model, or LIP model for short, which captures the center of mass dynamics of a real robot correctly when, throughout a step, the following conditions hold: (i) the center of mass (CoM) moves in a straight line; and (ii), the robot’s angular momentum about the center of

mass (L_c) is zero (or constant). This latter condition can be met by designing a robot to have light legs, such as the Cassie robot by Agility Robotics [8], or by deliberately regulating L_c to zero [9], [10]. When L_c cannot be regulated to a small value, an MPC feedback control law based on the LIP model has been proposed to minimize zero moment point (ZMP) tracking error and CoM jerk [11]–[13]. The effects of L_c can be compensated with ZMP, making a real robot’s CoM dynamics the same as those of a LIP [14]. Alternatively, L_c can be approximately predicted and used for planning [15], [16].

On the other hand, the control-centric approach called the Hybrid Zero Dynamics provides a mathematically-rigorous gait design and stabilization method for realistic bipedal models [17]–[26] without restrictions on robot or gait design. In this approach, the links/joints of the robot are synchronized via the imposition of “virtual constraints”, meaning the constraints are achieved through the action of a feedback controller instead of contact forces. As opposed to physical constraints, virtual constraints can be re-programmed on the fly. Like physical constraints, imposing a set of virtual constraints results in a reduced-dimensional model. The term “zero dynamics” for this reduced dynamics comes from the original work of [27], [28]. The term “hybrid zero dynamics” or HZD comes from the extension of zero dynamics to (hybrid) robot models in [29]. A downside of this approach, however, has been that it lacked the “analytical tractability” provided by the pendulum models¹, and it requires non-trivial time to find optimal virtual constraints for a realistic model.

While CoM velocity is the most widely used variable “to

¹The approaches in [30]–[32] to build reduced-order models via embeddings is a step toward attaching physical significance to the zero dynamic models.



Fig. 1: Cassie Blue, by Agility Robotics, on the iconic University of Michigan Wave Field.

Funding for this work was provided in part by the Toyota Research Institute (TRI) under award number No. 02281 and in part by NSF Award No. 1808051. All opinions are those of the authors.

The authors are with the College of Engineering and the Robotics Institute, University of Michigan, Ann Arbor, MI 48109 USA {ykgong, grizzle}@umich.edu

summarize the state” of a bipedal robot, angular momentum about the contact point has also been valued by multiple researchers. In [33], angular momentum is chosen to represent a biped’s state and it is regulated by stance ankle torque. In [34], the relative degree three property of angular momentum motivated its use as a state variable in the zero dynamics. In [35], [36], control laws for robots with an unactuated contact point were proposed to exponentially stabilize them about an equilibrium. In [23], angular momentum is explicitly used for designing nonholonomic virtual constraint. In [37], angular momentum is combined with the LIP model to yield a controller that stabilizes the transfer of angular momentum from one leg to the next through continuous-time (single-support-phase) control coupled with a hybrid model that captures impacts that occur at foot strike. In [38], the accuracy of the angular-momentum-based LIP model during the continuous phase is emphasized; as opposed to [37], angular momentum is allowed to passively evolve according to gravity during each single support phase, and foot placement is used to regulate the estimated angular momentum at the end of the ensuing step.

A. Objectives

The objectives of this paper are two-fold. Firstly, we seek to contribute insight on how pendulum models relate among one another and to the dynamics of a physical robot. We demonstrate that even when two pendulum models originate from the same (correct) dynamical principles, the approximations made in different coordinate representations lead to non-equivalent approximations of the dynamics of a (realistic) bipedal robot. Secondly, we seek a rapprochement of the most common pendulum models and the hybrid zero dynamics of a bipedal robot. Both of these objectives are addressed for planar robot models. The extension to 3D is not attempted here, primarily to keep the arguments as transparent as possible.

The first point that, approximations made in different coordinate representations lead to non-equivalent approximations of the dynamics of a real robot, is important in practice; hence we elaborate a bit more here, with details given in Sect. VI. Let’s only consider trajectories of a robot where the center of mass height is constant, and therefore, the velocity and acceleration of the center of mass height are both zero. In a realistic robot, the angular momentum about the center of mass, denoted by L_c , contributes to the longitudinal evolution of the center of mass, though it is routinely dropped in the most commonly used pendulum models. Can dropping L_c have a larger effect in one simplified model than another?

In the standard 2D LIP model, the coordinates are taken as the horizontal position and velocity of the center of mass *and the time derivative of L_c is dropped from the differential equation for the velocity*. It follows that the term being dropped is a high-pass filtered version of L_c , due to the derivative. Moreover, the derivative of L_c is directly affected by the motor torques, which are typically “noisy” (have high variance) in a realistic robot. On the other hand, in a less frequently used representation of a 2D inverted pendulum [23], [37]–[39], the coordinates are taken as angular momentum about

the contact point and the horizontal position of the center of mass, *and L_c is dropped from the differential equation for the position*. In this model, L_c (and not \dot{L}_c) shows up in the second derivative of the angular momentum about the contact point. It follows that variations in L_c are low-pass filtered in the second representation as opposed to high-pass filtered in the first, and thus, speaking intuitively, neglecting L_c should induce less approximation error in the second model. More quantitative results are shown in the main body of the paper.

In this paper, we focus on the underactuated single support phase dynamics and assume an instantaneous double support phase. The reader is referred to existing literature on how pendulum models [40], [41] and Hybrid Zero Dynamics [42]–[44] handle non-instantaneous double support phases; the topic is not discussed in this paper. We provide models for a robot with non-trivial feet. While most of the results are demonstrated for robots with point feet, we briefly show that the conclusions we obtained for robots with point feet still apply to robots with non-trivial feet. Further studies of how pendulum models and Hybrid Zero Dynamics handle non-trivial feet can be found in [11], [45]–[47]

B. Summary of Main Contributions

This paper makes the following contributions to pendulum models and zero dynamics:

- Starting from a common physically correct set of equations for real robots, we sequentially enumerate the approximations made to arrive at various reduced order pendulum models. This is done for bipedal robots with and without ankle torque.
- Several advantages of using angular momentum about the contact point as a key variable to summarize the dynamics of a bipedal robot are discussed and demonstrated.
- We show that a pendulum model parameterized by center of mass horizontal position and angular momentum about the contact point provides a higher fidelity representation of a physical robot than does the standard LIP model, which is a pendulum model parameterized by center of mass horizontal position and velocity. We identify the source of improvement as how the angular momentum about the center of mass is treated in the two models.
- For a set of non-holonomic virtual constraints, we derive the zero dynamics in a set of coordinates compatible with an angular-momentum-based pendulum model. We provide a precise sense in which the pendulum model is an approximation to the zero dynamics and demonstrate what this means for closed-loop stability of the full-order robot model.
- We formulate a foot placement strategy based on a high fidelity, one-step-ahead prediction of angular momentum about the contact point.
- We demonstrate that the resulting controller achieves highly dynamic gaits on a Cassie-series bipedal robot.

The last two contributions were introduced in [38] and are used here to demonstrate the utility of the proposed results. We will use both Rabbit [48] and Cassie Blue, shown in Fig. 1,

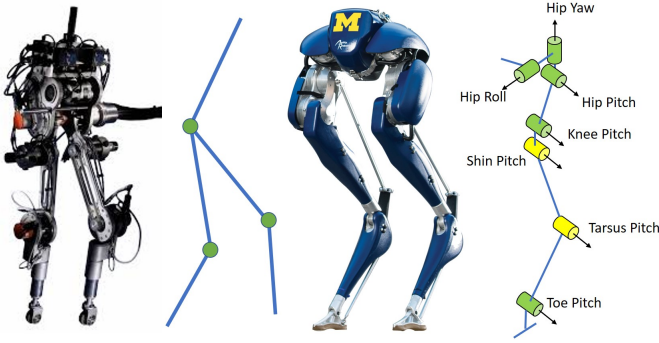


Fig. 2: Rabbit and Cassie. Rabbit is planar robot with 2 joints on each leg and Cassie is 3D robot with 7 joints on each leg.

to illustrate the developments in the paper. Experiments will be conducted exclusively on Cassie.

Rabbit is a 2D biped with five links, four actuated joints, and a mass of 32 Kg; see Fig. 2. Each leg weighs 10 kg, with 6.8 kg on each thigh and 3.2 kg on each shin. The Cassie robot designed and built by Agility Robotics weighs 32 Kg. It has 7 deg of freedom on each leg, 5 of which are actuated by motors and 2 are constrained by springs; see Fig. 2. A floating base model of Cassie has 20 degrees of freedom. Each foot of the robot is blade-shaped and provides 5 holonomic constraints when firmly in contact with the ground. Though each of Cassie’s legs has approximately 10 kg of mass, most of the mass is concentrated on the upper part of the leg. In this regard, the mass distribution of Rabbit is more typical of current bipedal robots seen in labs, which is why we include the Rabbit model in the paper.

C. Organization

The remainder of the paper is organized as follows. Sect. II introduces the full hybrid model of a bipedal robot with instantaneous double support phases. It also provides the robot’s center of mass dynamics in different coordinates. Sect. III summarizes several desirable properties of angular momentum about contact point. Sect. IV goes through the approximations that must be made to the center of mass dynamics in order to arrive at the most popular pendulum models. The approximation errors of the resulting pendulum models are analyzed and compared. Sect. V uses a one-step-ahead prediction of angular momentum to decide foot placement. This provides a feedback controller based on predicted angular momentum that will stabilize a 3D pendulum. Sect. VI provides background on a feedback control paradigm based on virtual constraints and the attendant zero dynamics. One of the pendulum models is shown to be a clear approximation to the zero dynamics, and the implications for stability analysis are discussed and illustrated by numerical computation. In Sect. VII, we design the virtual constraints for a Cassie-series bipedal robot. In Sect. VIII, we provide our path to implementing the controller on Cassie Blue. Additional virtual constraints are required beyond a path for the swing foot, and we provide “an intuitive” method for their design.

Sect. IX shows the results of experiments. Conclusion are give in Sect. X.

II. SWING PHASE AND HYBRID MODEL

This section introduces the full-dimensional swing-phase model that describes the mechanical model when the robot is supported on one leg and a hybrid representation used for walking that captures the transition of support legs. The section concludes with a summary of a few model properties that are ubiquitous when discussing low-dimensional pendulum models of walking.

A. Full-dimensional Single Support Model

We assume a planar bipedal robot satisfying the specific assumptions in [17, Chap. 3.2] and [34], which can be summarized as a revolute point contact with the ground, no slipping, all other joints are independently actuated, and all links are rigid and have mass. The gait is assumed to consist of alternating phases of single support (one “foot” on the ground), separated by instantaneous double support phases (both feet in contact with the ground), with the impact between the swing leg and the ground obeying the non-compliant, algebraic contact model in [49], [50] (see also [17, Chap. 3.2]).

The contact point with the ground, which we refer to as the stance ankle, can be passive or actuated. Even when actuated, the stance ankle is “weak” in the sense that only limited torque can be applied before the foot rolls about one of its extremities. The swing ankle is not weak, however, because it only needs to regulate the orientation of the swing foot. To accommodate both actuation scenarios, we will routinely separate the stance ankle actuation from other actuators on the robot so that it can be either set to zero or appropriately exploited.

We assume a world frame (x, z) with the right-hand rule. We assume the swing-phase (pinned) Lagrangian model is derived in coordinates $q := (q_0, q_1, \dots, q_n) \in Q$, where q_0 is an absolute angle (referenced to the z -axis of the world frame) and $q_b := (q_1, \dots, q_n)$ are body coordinates. Furthermore, we reference the contact point (i.e., stance ankle) to the origin of the world frame.

With the above sets of assumptions, the robot in single-support is either fully actuated or has one degree of under-actuation. Moreover, q_0 is a cyclic variable (of the kinetic energy). It follows that the dynamic model can be expressed in the form

$$D(q_b)\ddot{q} + C(q, \dot{q})\dot{q} + G(q) = B(q)u, \quad (1)$$

where the vector of motor torques $u \in \mathbb{R}^n$ and the torque distribution matrix has full column rank. The model is written in state space form by defining

$$\dot{x} = \begin{bmatrix} \dot{q} \\ D^{-1}(q_b) [-C(q, \dot{q})\dot{q} - G(q) + B(q)u] \end{bmatrix} \quad (2) \\ =: f(x) + g(x)u$$

where $x := (q; \dot{q})$. The state space of the model is $\mathcal{X} = TQ$. For each $x \in \mathcal{X}$, $g(x)$ is a $2(n+1) \times (n+1)$ matrix. In natural coordinates $(q; \dot{q})$ for TQ , g is independent of \dot{q} .

B. Full Dimensional Hybrid Model

In the above, we implicitly assumed left-right symmetry in the robot so that we could avoid the use of two single-support models—one for each leg playing the role of the stance leg—by relabeling the robot’s coordinates at impact, thereby swapping their roles. Immediately after swapping, the former swing leg is in contact with the ground and is poised to take on the role of the stance leg. The result of the impact and the relabeling of the states provides an expression

$$x^+ = \Delta(x^-) \quad (3)$$

where $x^+ := (q^+; \dot{q}^+)$ (resp. $x^- := (q^-; \dot{q}^-)$) is the state value just after (resp. just before) impact and

$$\Delta(x^-) := \begin{bmatrix} \Delta_q(q^-) \\ \Delta_{\dot{q}}(q^-) \dot{q}^- \end{bmatrix}. \quad (4)$$

A detailed derivation of the impact map is given in [17], showing that it is linear in the generalized velocities.

A hybrid model of walking is obtained by combining the single support model and the impact model to form a system with impulse effects [51]. A non-instantaneous double support phase can be added [42], [44], but we choose not to do so here. Even though the mechanical model of the robot is time-invariant, we will allow feedback controllers for (2) that are time varying. So that the hybrid model in closed loop can be analyzed with tools developed for time-invariant hybrid systems, we do the standard “trick” of adding time as a state variable via $\dot{\tau} = 1$. The guard condition (aka switching set) for terminating a step is

$$\mathcal{S} := \{(q, \dot{q}) \in T\mathcal{Q} \mid p_{\text{sw}}^z(q) = 0, \dot{p}_{\text{sw}}^z(q, \dot{q}) < 0\}, \quad (5)$$

where $p_{\text{sw}}^z(q)$ is the vertical height of the swing foot. It is noted that \mathcal{S} is independent of time. Combining (2), (3) with the guard set and time gives the hybrid model

$$\Sigma : \begin{cases} \dot{x} = f(x) + g(x)u & x^- \notin \mathcal{S} \\ \dot{\tau} = 1 \\ x^+ = \Delta(x^-) & x^- \in \mathcal{S} \\ \tau^+ = 0. \end{cases} \quad (6)$$

It is emphasized that the guard condition for re-setting the “hybrid time variable”, τ , is determined by foot contact.

C. Center of Mass Dynamics in Single Support

While (2) is typically high dimensional and nonlinear, standard mechanics yields simpler equations for the evolution of the center of mass. For succinctness, we only consider the planar case and define the following variables:

- (x_c, z_c) : CoM position in the frame of the contact point.
- v_c : CoM velocity in x -direction. The velocity in z -direction is denoted by \dot{z}_c
- L_c : y -component of Angular momentum about CoM.
- L : y -component of Angular momentum about contact point.
- u_a : ankle torque at the contact point.

In addition, we note the following (standard) result

$$L = L_c + m \begin{bmatrix} x_c \\ z_c \end{bmatrix} \wedge \begin{bmatrix} \dot{x}_c \\ \dot{z}_c \end{bmatrix} \quad (7)$$

where \wedge is the 2D version of cross product

$$\begin{bmatrix} x_c \\ z_c \end{bmatrix} \wedge \begin{bmatrix} \dot{x}_c \\ \dot{z}_c \end{bmatrix} := \left(\begin{bmatrix} x_c \\ 0 \\ z_c \end{bmatrix} \times \begin{bmatrix} \dot{x}_c \\ 0 \\ \dot{z}_c \end{bmatrix} \right) \cdot \begin{bmatrix} 0 \\ 1 \\ 0 \end{bmatrix}.$$

We refer to (7) as the *angular momentum transfer formula* because it relates angular momentum determined about two different points.

In the following, we provide the CoM dynamics for two sets of coordinates

- (x_c, v_c)
- (x_c, L) , and
- (θ_c, L) ,

where

$$\theta_c := \text{atan}(x_c/z_c) \quad (8)$$

and we assume that $z_c > 0$. We will subsequently dedicate Sect. IV to establishing connections between pendulum models and zero dynamics, which will allow the zero dynamics to be intuitively grounded in physics.

Case 1: (x_c, v_c) Horizontal Position and Velocity Differentiating (7) and using $v_c = \dot{x}_c$ results in

$$\begin{aligned} \dot{x}_c &= v_c \\ \dot{v}_c &= \frac{g}{z_c} x_c + \frac{\ddot{z}_c}{z_c} x_c - \frac{\dot{L}_c}{m z_c} + \frac{u_a}{m z_c}. \end{aligned} \quad (9)$$

In general, z_c depends on q , \dot{z}_c and L_c depend on both q and \dot{q} . While \dot{L}_c and \ddot{z}_c depend on q , \dot{q} , and the motor torques u , it is more typical to replace the motor torques by the ground reaction forces. In particular, one uses $\ddot{z} = g - \frac{1}{m} F_z$ and $\dot{L}_c := \frac{d}{dt} L_c = x_c F_z - z_c F_x + u_a$, where F_x and F_z are the horizontal and vertical components of the ground reaction forces. In turn, the ground reaction forces can be expressed as functions of q , \dot{q} , and the motor torques, u .

Case 2: (x_c, L) Angular Momentum and Horizontal Position: Manipulating (7) and using $\dot{L} = mgx_c + u_a$ results in

$$\begin{aligned} \dot{x}_c &= \frac{L}{m z_c} + \frac{\dot{z}_c}{z_c} x_c - \frac{L_c}{m z_c} \\ \dot{L} &= mgx_c + u_a. \end{aligned} \quad (10)$$

The remarks made above on z_c , \dot{z}_c , and L_c apply here as well.

Case 3: (θ_c, L) Alternative absolute angle (cyclic variable): Differentiating (8) yields

$$\dot{\theta}_c = \frac{L - L_c}{m r_c^2(q_b)}. \quad (11)$$

Combining (7) and (11) yields

$$\begin{aligned} \dot{\theta}_c &= \frac{L - L_c}{m r_c^2} \\ \dot{L} &= m g r_c \sin(\theta_c) + u_a. \end{aligned} \quad (12)$$

It is remarked that the derivatives of the generalized coordinates only appear through L_c . In the following, we will keep the discussion primarily focused on (10), but most of the results apply to (12) as well; see Appendix A.

III. ANGULAR MOMENTUM ABOUT CONTACT POINT

In this paper, we are focusing on the angular momentum about the contact point, L , as a replacement for the center of mass velocity, v_c , which is used as an indicator of walking status in many other papers [7], [26], [52], [53]. Specific to this paper, L is also a state of the zero dynamics. Before we proceed to that, it is beneficial to explain why L can replace v_c , summarize some general properties of L , and highlight some of its advantages versus v_c . More specific advantages of using L in the zero dynamics and the LIP model will be discussed in later sections.

We first need to answer why L can replace v_c as an indicator of walking. The relationship between angular momentum and **linear momentum** for a 3D bipedal robot is

$$L = L_c + p_c \wedge m v_c, \quad (13)$$

where L_c is the angular momentum about the center of mass, v_c is the linear velocity of the center of mass, m is the total mass of the robot, and p_c is the vector emanating from the contact point to the center of mass.

For a bipedal robot that is walking instead of doing somersaults, it is reasonable to focus on gaits where the angular momentum about the center of mass oscillate about zero (e.g., arms are not rotating as in a flywheel). The oscillating property of L_c is discussed in [54], [55]. When L oscillates about zero, (13) implies that the difference between L and $p_c \wedge m v_c$ also oscillates about zero, which we will write as

$$L - p_c \wedge m v_c = L_c \text{ oscillates about } 0. \quad (14)$$

From (14), we see that we approximately obtain a desired linear velocity by regulating L . Hence, in walking robots without a flywheel, one can replace the control of linear velocity with control of angular momentum about the contact point.

What are there advantages to using L ?

- (a) The first advantage of controlling L is that it provides a more comprehensive representation of current walking status because it is the sum of angular momentum about the center of mass, L_c , and linear momentum, $p_c \wedge m v_c$. From (9), we see that there exists momentum transfer between these two quantities. If L_c increases, it must “take” some momentum away from v_c , and vice versa. For normal bipedal walking, L_c oscillates about zero. L_c functions to store momentum [56], but importantly it can only store it for a short amount of time. When designing a foot placement strategy, it is important to take the “stored” momentum into account.

When balancing on one foot for example, some researchers plan L_c and v_c separately [57], or use L_c as an input to regulate balance by waving the torso, arms, or swing leg [58], [59] or even a flywheel [60]. Here, instead of moving limbs to generate a certain value of L_c , we view L_c as a result of the legs and torso moving to fulfill other tasks. In this paper, we observe L_c and take it into consideration through L and do not seek to regulate it directly as an independent quantity.

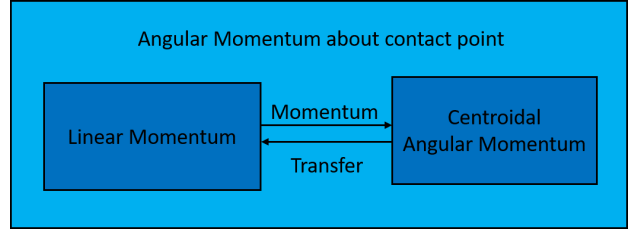


Fig. 3: The relation between L , L_c , and v_c^x . Equation (13) shows L is the sum of L_c and a term that is linear in v_c , while the second line of (9) shows the transfer of momentum between L_c and v_c . The relation is an analogue of mechanical, kinetic and potential energy.

- (b) Secondly, because $\dot{L} = mgx_c + u_a$ depends only on the CoM position, it follows that L has relative degree three with respect to all inputs except the stance ankle torque, where it has relative degree one. Consequently, the evolution L is only weakly affected by motor torques of the body, that is u_b , during a step. In Fig. 4 (a) and (d) and Fig. 5 (a) we see that the trajectory of L consistently has a convex shape when stance ankle torque is zero, irrespective of model or speed. We’ll see later the same property in experimental data.
- (c) The discussion so far has focused on the single support phase of a walking gait. Bipedal walking is characterized by the transition between left and right legs as they alternately take on the role of stance leg (aka support leg) and swing leg (aka non-stance leg). In double support, the transfer of angular momentum between the two contact points satisfies

$$L_2 = L_1 + p_{2 \rightarrow 1} \wedge m v_c, \quad (15)$$

where $p_{2 \rightarrow 1}$ is the vector from point 2 (the new stance leg position) to point 1 (the previous stance leg position). Hence, the change of angular momentum between two contact points depends only on the vector defined by the two contact points and the center of mass velocity. In particular, angular momentum about a given contact point is invariant under the impulsive force generated at that contact point. Consequently, we can easily determine the angular momentum about the new contact point by (15) when impact happens without resorting to approximating assumptions about the impact model. Moreover, if \dot{z}_c is zero and the ground is level, then $p_{2 \rightarrow 1} \wedge m v_c = 0$, and hence $L_2 = L_1$. We note that pendulum models parameterized with CoM velocity often assume continuity at impact, which is not generally true for real robots.

Figure 4 shows the evolution of L , v_c , L_c and \dot{L}_c during a step for both Cassie and Rabbit, when walking speed is about 2 m/s, $\dot{z}_c = 0$, and no stance ankle torque is applied. Figure 5 shows the evolution of L , v_c , L_c for Rabbit walking at a range of speeds from -1.8 m/s to 2.0 m/s. Figure 4 and 5 also show the continuity property of L at impact.

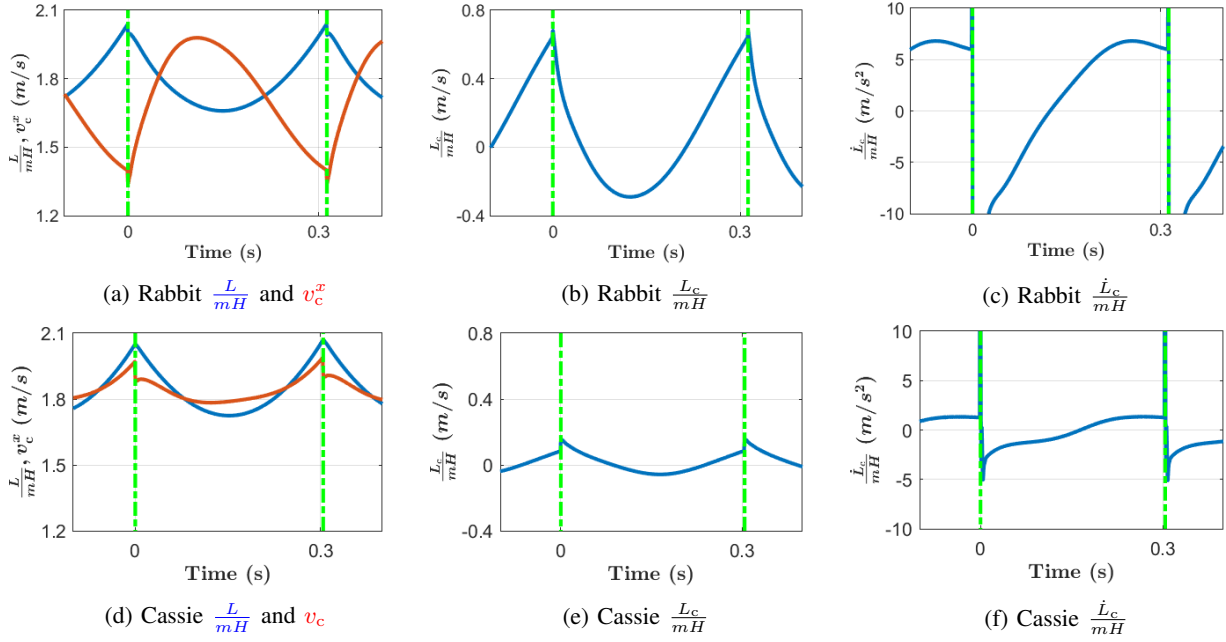


Fig. 4: Plots of L , v_c , and \dot{L}_c for the bipedal robots Rabbit and Cassie walking at about 2m/s, while z_c is carefully regulated to 0.6m. The vertical green lines indicate the moment of impact. For both robots, the angular momentum about the contact point, L , has a convex shape (due to $\dot{L} = mgx_c + u_a$, $u_a = 0$ and CoM passes the contact point only once), similar to the trajectory of a LIP model, while the trajectory of the longitudinal velocity of the center of mass, v_c , has no consistent shape. The variation of L_c throughout a step, which is caused by the legs of the robot having mass, is what leads to a difference in the CoM velocity between a real robot and a LIP model. The patterns of L_c shown above are not specific to certain robot or controller but match the walking mechanism described in [54], [55]. In this figure, L is continuous at impact, which is based on two conditions: $v_c^z = 0$ at impact and the ground is level. Even when these two conditions are not met, the jump in L at impact can be easily calculated with (15).

IV. COMPARISON OF APPROXIMATE MODELS FOR CENTER OF MASS DYNAMICS

Each of the dynamical models (9), (10), and (12) is valid along all trajectories of the full-dimensional model. This section systematically goes through the models in Sec. II-C and looks for connections with low-dimensional pendulum models. Subsequently, Sect. VI makes connections between pendulum models and the zero dynamics.

A. Constant Pendulum Height

If CoM height is constant, i.e., $z_c = H$, $\dot{z}_c = 0$, and $\ddot{z}_c = 0$, then (9) and (10) become

$$\begin{aligned} \dot{x}_c &= v_c \\ \dot{v}_c^x &= \frac{g}{H}x_c - \frac{\dot{L}_c}{mH} + \frac{u_a}{mH}, \end{aligned} \quad (16)$$

and

$$\begin{aligned} \dot{x}_c &= \frac{L}{mH} - \frac{L_c}{mH} \\ \dot{L} &= mgx_c + u_a, \end{aligned} \quad (17)$$

respectively. Equation (17) can be rewritten as

$$\begin{aligned} \dot{x}_c &= v_p - \frac{L_c}{mH} \\ \dot{v}_p &= \frac{g}{H}x_c + \frac{u_a}{mH}, \end{aligned} \quad (18)$$

where $v_p = \frac{L}{mH}$, which is more directly comparable to (16). In this paper we frequently plot L scaled by the coefficient $\frac{1}{mH}$, so that it can be more directly compared to v_c (same units and similar magnitudes).

At this point, no approximations have been made and both models are valid everywhere that $z_c(q) \equiv H$. Hence, the two models are still *equivalent* representations of the center of mass dynamics for all trajectories satisfying $z_c(q) \equiv H$. *We'll next argue that the models are not equivalent when it comes to approximations.*

Dropping the \dot{L}_c term in (16) results in:

$$\begin{aligned} \dot{x}_c &= v_c \\ \dot{v}_c &= \frac{g}{H}x_c + \frac{u_a}{mH}. \end{aligned} \quad (19)$$

This is the well-known LIP model proposed by [61].

Dropping L_c in (17) results in

$$\begin{aligned} \dot{x}_c &= \frac{L}{mH} \\ \dot{L} &= mgx_c + u_a, \end{aligned} \quad (20)$$

which is used in [37], [38]. In [37], (20) is used instead of (19) so that the easy ‘‘update’’ property of L at impact can be used. In this paper, we demonstrate that during the continuous phase, the states of (20) much more accurately capture the evolution of (x_c, L) in a real robot than the states of (19) capture the evolution of (x_c, v_c) . Moreover, we will make

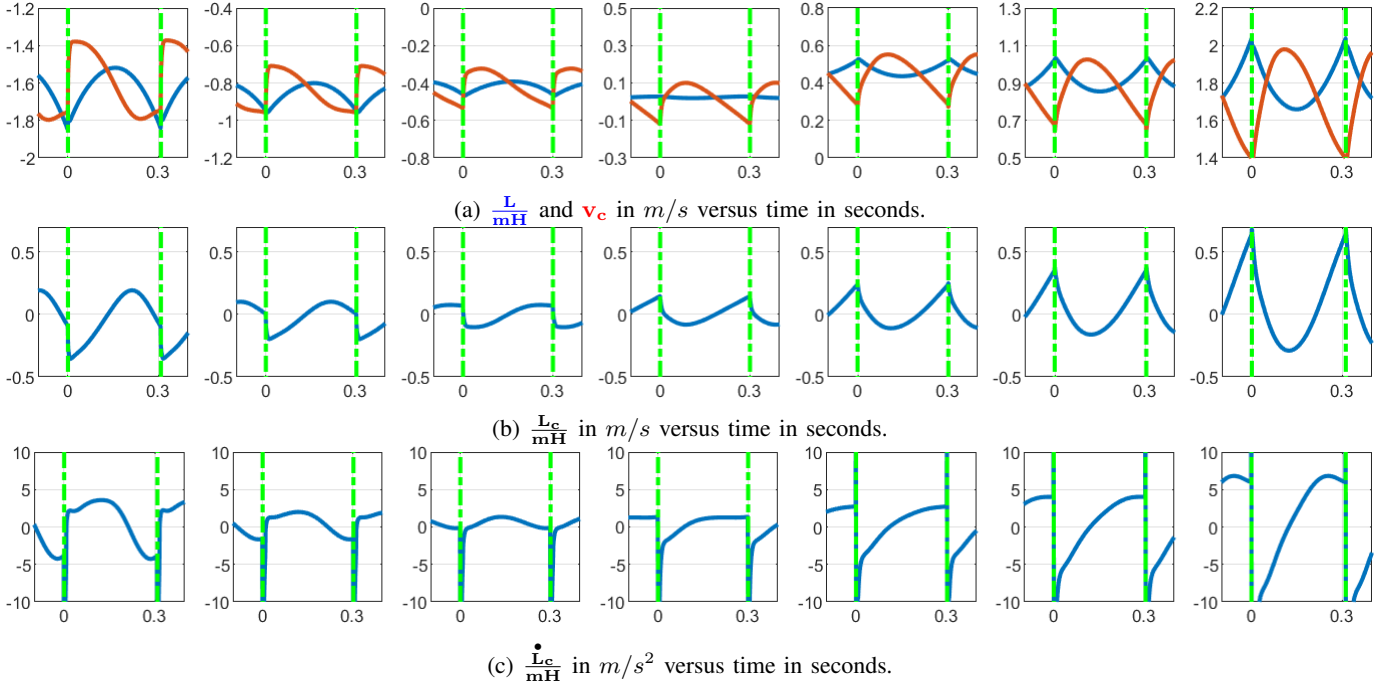


Fig. 5: Plots of L , v_c , and \dot{L}_c for Rabbit walking at different speeds. The green vertical lines indicate the moment of impact. (a) shows that L always has a convex or concave shape like the LIP model, while v_c has no determinant shape. The shape of L is a direct consequence of $\dot{L} = mgx_c$. The quantities $\frac{L}{mH}$ and v_c are close in scale and oscillate about one another. This shows that directly regulating L does indeed indirectly regulate v_c . (b) and (c) show the scales of L_c and \dot{L}_c . It is seen that \dot{L}_c is much larger in scale and thus omitting it in (16) can create a larger error than neglecting L_c in (17).

use of this improved accuracy in the design of a feedback controller. To distinguish the model (20) from (19), we will denote it by ALIP, where A stands for Angular Momentum.

For a robot with a point mass, the two models (19) and (20) are equivalent, because L_c is then identically zero. For a real robot with L_c and \dot{L}_c that are nonnegligible, however, we argue that (20) is more accurate than (19) primarily because of three properties,

- (a) **Relative Amplitude.** Based on our observations, the ratio of \dot{L}_c/mgx_c is much larger than L_c/L over a wide range of walking velocities; thus the simplification (20) introduces relatively less error than (19).
- (b) **Relative degree.** L has relative degree two with respect to L_c and three with respect to \dot{L}_c , whereas v_c has relative degree one with respect to \dot{L}_c . Because integration is a form of low-pass filtering, the lower relative degree makes v_c more sensitive to the omission of the L_c term.
- (c) L_c oscillates about zero. What makes (20) even more accurate is that, based on our own observation and references [54], [55], the sagittal plane component of L_c oscillates about zero for periodic and non-periodic gaits. The oscillation of L_c results in the effect of L_c on x_c roughly averaging out to zero over a step.

In Fig. 6, we have used the models (19) and (20) to predict the values of v_c and L at the end of a step. We plot $\frac{L}{mH}$ instead of L to make the scale and units comparable. The blue line is the true trajectory of L (resp. v_c) during a step. The red line shows the prediction of L (resp. v_c) at the end of each of step,

at each moment throughout a step, based on the instantaneous values of x_c and L (v_c) at that moment. The red line would be perfectly flat if (20) and (19) perfectly captured the evolution of L (v_c), respectively, in the full simulation model, and the flatter the estimate, the more faithful is the representation.

The prediction errors of (19) and (20) caused by neglecting L_c and \dot{L}_c , respectively, satisfy

$$\begin{aligned} \dot{x}_e &= v_e \\ \dot{v}_e &= \frac{g}{H}x_e - \frac{\dot{L}_c}{mH}, \end{aligned} \quad (21)$$

and

$$\begin{aligned} \dot{x}_e &= \frac{L_e}{mH} - \frac{L_c}{mH} \\ \dot{L}_e &= mgx_e, \end{aligned} \quad (22)$$

where (x_e, L_e) are the differences in the trajectories of (19) and (18); similarly, (x_e, v_e) are the differences in the trajectories of (20) and (16). Direct solution of these two sets of differential equations for zero initial conditions leads to

$$\begin{aligned} v_e(t_2, t_1) &= e_1(t_2, t_1) \\ &= e_2(t_2, t_1) + e_3(t_2, t_1) \end{aligned} \quad (23)$$

$$\frac{L_e(t_2, t_1)}{mH} = e_2(t_2, t_1), \quad (24)$$

where

$$\begin{aligned} e_1(t_2, t_1) &= -\frac{1}{mH} \int_{t_1}^{t_2} \cosh(\ell(t_2 - \tau)) \dot{L}_c(\tau) d\tau \\ e_2(t_2, t_1) &= -\frac{1}{mH} \int_{t_1}^{t_2} \ell \sinh(\ell(t_2 - \tau)) L_c(\tau) d\tau \\ e_3(t_2, t_1) &= -\frac{1}{mH} (L_c(t_2) - \cosh(\ell(t_2 - t_1)) L_c(t_1)). \end{aligned}$$

Figure 7 shows the (relative) sizes of these error terms. If we view L_c as a disturbance and prediction error as an output in (21) and (22), we obtain the corresponding Laplace transforms and Bode plots shown in Fig. 8.

B. Simulation Comparison

We compare controllers designed on the basis of the ALIP and LIP models in simulation. The results shown in Fig 9 demonstrate the advantage of using ALIP over LIP for controller design. The initial hip velocity is set to 0.5 m/s and hip position is centered over the contact point. The goal of each controller is to regulate v_c (resp., L) to zero, with foot placement as the decision variable and step duration constant. In the plots, we observe that the ALIP-based controller regulates L closely to zero and thus has an average v_c close to zero, while the LIP-based controller is unable to regulate v_c effectively. The reason is that, at the end of a step, the linear momentum was transferred to centroidal angular momentum L_c due to the movement of Rabbit’s heavy legs (see Eqn (18)), resulting in a small v_c , which misleads the LIP controller into choosing a small foot displacement. In the ALIP model, L is less affected by momentum transfer between v_c and L_c because L captures their sum, and thus the ALIP model suggests better foot placement. Though with a LIP controller it is possible to regulate velocity through ZMP (ankle torque) during continuous phase, we argue that with an ALIP controller, the capability of ZMP can be reserved for better purposes than compensating for model error.

C. Non-zero Ankle Torque

In previous subsections we have demonstrated the accuracy of pendulum model parameterized with L when ankle torque is zero. According to Eqn (10), the effect of L_c and u_a on the system are independent due to the superposition property. So if dropping L_c term has little effect on the model accuracy when u_a is zero, it should still has little effect on the model accuracy when u_a is non-zero. Though L_c trajectory itself will be changed when u_a is non-zero, its pattern is still similar. Here for completeness we run a simulation on Rabbit. The results are shown in Fig. 10

V. STABILIZING THE ALIP MODEL

In this section, we provide a means to regulate angular momentum about the contact point to approximately achieve a desired walking speed. Specifically, the ALIP model (20) is

used to form a one-step ahead prediction of angular momentum, L . In combination with the angular momentum transfer formula (15), a feedback law results for where to place the swing foot at the end of the current step so as to achieve a desired angular momentum at the end of the ensuing step. In robot locomotion, this is typically called “foot placement control” [7], [62]–[64].

L can also be controlled through vertical CoM velocity at the end of a step [37], adjusting the step duration [61], [65], ankle torque during continuous phase [33], which has a relative degree one relation to L , or by other torques applied at the body coordinates during the continuous single support phase [35], [36], [66], which have a relative degree three relation to L . We summarize these general methods² to regulate L in Table I.

Continuous Phase	
Relative Degree Three	L_c, z_c
Relative Degree One	u_a
Transition Event	
Initial condition for next continuous phase	$x_c(0), L(0)$
Phase duration	Step Time

TABLE I: Methods to regulate L for walking.

A. Gait assumptions

When designing the foot placement controller, we assume the gait of the robot is controlled such that:

- the height of the center of mass is constant, that is $z_c \equiv H > 0$;
- each step has constant duration $T > 0$; and
- a desired swing leg horizontal position, $p_{sw \rightarrow CoM}^{x, des}$, can be achieved at the end of the step.

We’ll explain how to accomplish these objectives via the method of virtual constraints in Sections VI and VII.

B. Notation

We distinguish among the following time instances when specifying the control variables.

- T is the step time.
- T_k is the time of the k th impact and thus equals kT .
- T_k^- is the end time of step k , so that
- T_k^+ is the beginning time of step $k + 1$ and T_{k+1}^- is the end time of step $k + 1$.
- $(T_k^- - t) = (T - \tau(t))$ is the time until the end of step k .

The superscripts $+$ and $-$ on T_k are necessary because of the (potential) jump in a trajectory’s values from the impact map; see [67]. As shown in Fig. 11, $x(T_k^-)$ is the limit from the left of the model’s solution at the time of impact, in other words

²With the exception of the method based on regulating L_c , each of the methods listed in Table I can be applied to a pendulum model parameterized with L . For humans, L_c is mainly utilized when we are about to fall off a support structure, such as when balancing on a tightrope. In bipedal robots without a flywheel, the effect of L_c on L is weak, due to multiple factors such as kinematic constraints, torque limits, and being relative degree three with respect to body torques. L_c is an ineffective means of regulating L for the same reasons that dropping L_c in the ALIP model does not introduce significant inaccuracy.

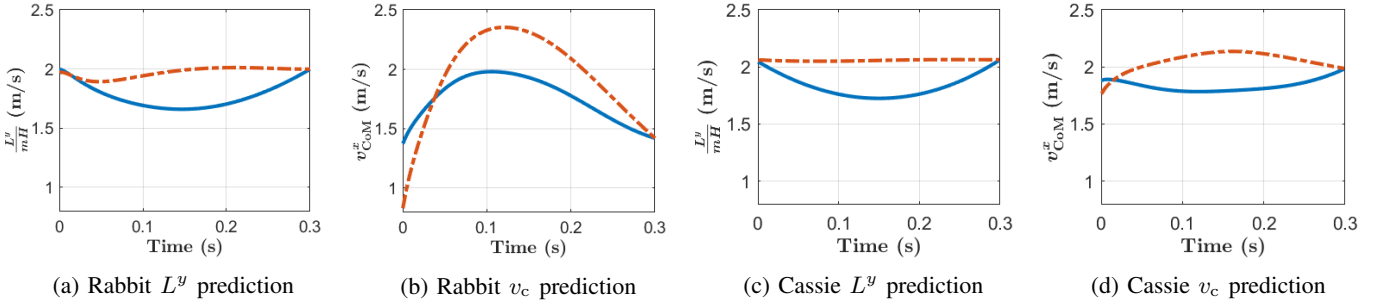


Fig. 6: Comparison of the ability to predict velocity vs angular momentum at the end of a step. The instantaneous values are shown in **blue** and the predicted value at the end of the step is shown in **red**, where a perfect prediction would be a flat line that intercepts the terminal point of the blue line. The most crucial decision in the control of a bipedal robot is where to place the next foot fall. In the standard LIP controller, the decision is based on predicting the longitudinal velocity of the center of mass. In Sect. V we use angular momentum about the contact point. We do this because on realistic bipeds, a LIP-style model provides a more accurate and reliable prediction of L than v_c . The comparison is more significant on Rabbit, whose leg center of mass is further away from the overall center of mass.

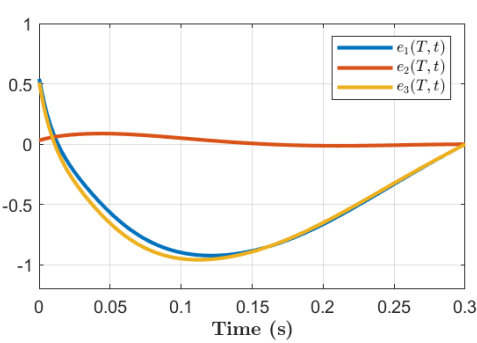


Fig. 7: A plot of the error terms in (23) and (24) resulting from dropping \dot{L}_c and L_c , respectively, for the Rabbit model walking at 2 m/s. The take-home message is that of the terms $e_2(t_1, t_2) + e_3(t_1, t_2)$ in (23) comprising the velocity error of the LIP model, the term $e_3(t_1, t_2)$ shown in the **yellow** line contributes by far the largest portion of the total error shown by the **blue** line. The error of the ALIP model, however, is given only by $e_2(t_1, t_2)$, which results in the significantly reduced prediction error shown by the **red** line.

it's value “just before” impact, while $x(T_K^+)$ is the limit from the right of the model's solution at the time of impact, in other words it's value “just after” impact.

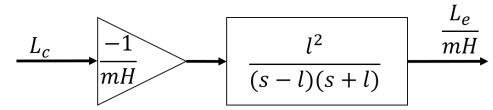
With this notation, the reset map for the ALIP becomes

$$\begin{aligned} x_c(T_k^+) &= p_{sw \rightarrow CoM}^x(T_k^-) \\ L(T_k^+) &= L(T_k^-), \end{aligned} \quad (25)$$

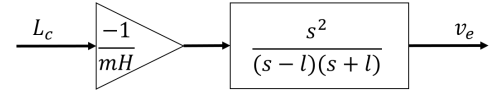
after noting that (15) simplifies to L being constant across impacts when the ground is level and the vertical velocity of the center of mass is zero.

We remind the reader that

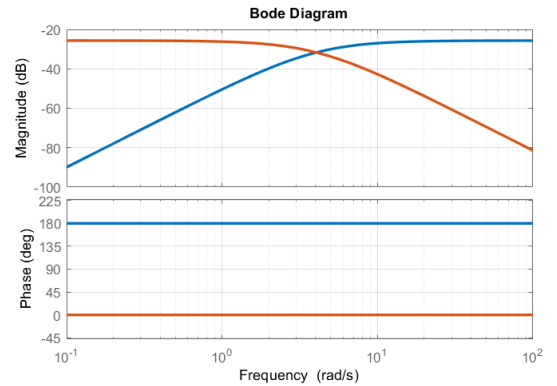
- $p_{st \rightarrow CoM}$, $p_{sw \rightarrow CoM}$ are the vectors emanating from stance/swing foot to the robot's center of mass. The stance foot defines the current contact point, while the swing foot is defining the point of contact for the next impact and is therefore a control variable.
- Also, for the implementation of the control law on the 3D biped Cassie in Sect. VII, we need to distinguish between



(a) ALIPM



(b) LIPM



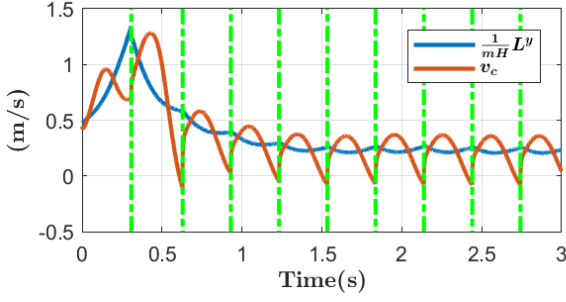
(c) Bode Plot

Fig. 8: How neglecting L_c and \dot{L}_c generates errors in ALIPM and LIPM. Note the low-pass (ALIPM in **red**) vs high-pass (LIPM in **blue**) nature of the respective transfer functions.

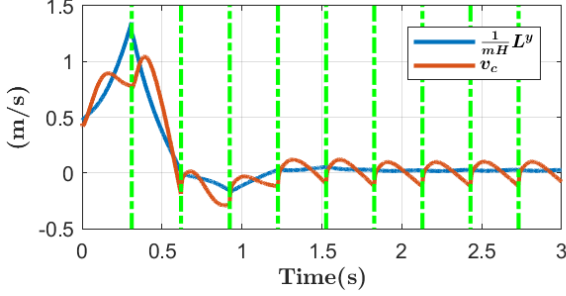
L^y and L^x , the y and x components of the angular momentum (sagittal and frontal planes), respectively.

C. Foot placement in longitudinal direction

The control objective will be to place the swing foot at the end of the current step so as to achieve a desired value of angular momentum at the end of the ensuing step. The need to regulate the angular momentum one-step ahead of the current step, instead of during the current step, is because in (20) L is



(a) LIP controller



(b) ALIP controller

Fig. 9: Simulation results of Rabbit with controllers based on LIP and ALIP, following an identical design philosophy, based on foot placement. The details of the controller are described in Sec V and Sec VII. The controller based on the ALIP model is much more effective in regulating velocity to zero.

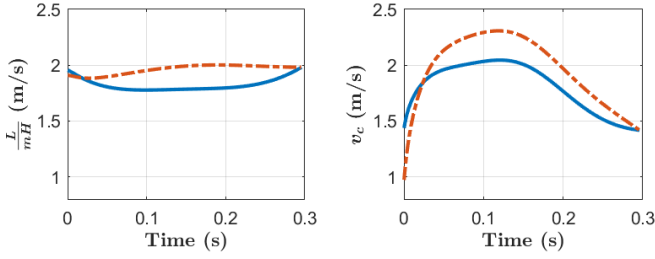
(a) Rabbit L prediction(b) Rabbit v_c prediction

Fig. 10: Comparison of the ability to predict velocity vs angular momentum at the end of a step in a model with ankle torque $u_a = 30 \sin(2\pi\tau/T)$, where τ varies from 0 to T during a step. The instantaneous values are shown in blue and the predicted value at the end of the step is shown in red. Because ankle torque is an input, we assume its trajectory is known when making predictions. For comparison purposes with Fig. 6, the ankle torque is chosen to be sufficiently large so that gravity is no longer dominant in $\dot{L} = mgx_c + u_a$ and the trajectory of L is no longer convex.

passive without ankle torque, in other words, it is not affected by the control actions of the current step. The only way to act on its states is through the transition events.

The closed-form solution of (20) at time T and initial time t_0 is

$$\begin{bmatrix} x_c(T) \\ L^y(T) \end{bmatrix} = A(T - t_0) \begin{bmatrix} x_c(t_0) \\ L^y(t_0) \end{bmatrix}, \quad (26)$$

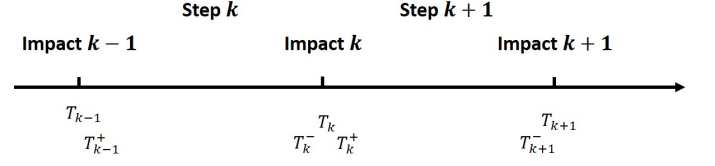


Fig. 11: For a given time, T_k , the notation T_k^- means that we are evaluating a function as a limit from the left of T_k , while T_k^+ means we are taking a limit from the right. This is compatible with how trajectories are defined for the hybrid model (6).

where

$$A(t) = \begin{bmatrix} \cosh(\ell t) & \sinh(\ell t)/(mH\ell) \\ mH\ell \sinh(\ell t) & \cosh(\ell t) \end{bmatrix}$$

and $\ell = \sqrt{\frac{g}{H}}$.

In the following, we breakdown the evolution of L^y from t to T_{k+1}^- , for three key time intervals or instances with the aim of forming a one-step-ahead estimate of angular momentum about the contact point.

1) From t to T_k^- : From the second row of (26), an estimate for the angular momentum about the contact point at the end of current step, $\hat{L}^y(T_k^-, t)$, can be continuously updated by

$$\begin{aligned} \hat{L}^y(T_k^-, t) = & mH\ell \sinh(\ell(T_k^- - t))x_c(t) \\ & + \cosh(\ell(T_k^- - t))L^y(t). \end{aligned} \quad (27)$$

Forming the running estimate in (27), versus a fixed estimate based on the values of x_c and L^y at the beginning of the step, allows disturbances to be taken into account.

2) From T_k^- to T_k^+ : This involves applying the reset map (25), yielding

$$x_c(T_k^+) = p_{\text{sw} \rightarrow \text{CoM}}^x(T_k^-) \quad (28)$$

$$\hat{L}^y(T_k^+, t) = \hat{L}^y(T_k^-, t). \quad (29)$$

3) From T_k^+ to T_{k+1}^- : Similar to (27), the angular momentum at the end of the next step is estimated by

$$\hat{L}^y(T_{k+1}^-, t) = mH\ell \sinh(\ell T)x_c(T_k^+, t) + \cosh(\ell T)\hat{L}^y(T_k^+, t). \quad (30)$$

Solving (27)-(30) so that

$$\hat{L}^y(T_{k+1}^-, t) = L^{y \text{ des}},$$

a desired value of angular momentum at the end of a step, (which can be obtained by $L^{y \text{ des}} = mHv^{x \text{ des}}$), yields a formula for the desired swing foot position at the end of the current step, given the value of desired angular momentum at the end of the next step,

$$p_{\text{sw} \rightarrow \text{CoM}}^{x \text{ des}}(T_k^-, t) := \frac{L^{y \text{ des}} - \cosh(\ell T)\hat{L}^y(T_k^-, t)}{mH\ell \sinh(\ell T)}. \quad (31)$$

Remark: Instead of the deadbeat control (31), it is possible to asymptotically approach a desired value of L^{des} with the control law

$$\begin{aligned} p_{\text{sw} \rightarrow \text{CoM}}^{x \text{ des}}(T_k^-, t) := & \frac{1 - \alpha}{mH\ell \sinh(\ell T)} L^{y \text{ des}} \\ & + \frac{\alpha - \cosh(\ell T)}{mH\ell \sinh(\ell T)} \hat{L}^y(T_k^-, t), \end{aligned} \quad (32)$$

which achieves

$$(L^{y \text{ des}} - \widehat{L}^y(T_{k+1}^-, t)) = \alpha(L^{y \text{ des}} - \widehat{L}^y(T_k^-, t)) \quad (33)$$

for $\alpha \in [0, 1)$. Hence, for $\alpha = 0$, (32) reduces to (31).

D. Stability Analysis of the ALIP for L^{des}

Consider the ALIP model (20) with zero ankle torque and rest map (25). To compute the Poincaré map, we take the Poincaré section as $S := \{(x_c, L, \tau) \mid \tau = 0^+\}$, which is the set of states just after impact. Computing (20) over one step and using swing foot position with respect to the center of mass, u_{fp} , as an input, yields,

$$\begin{bmatrix} x_c(T^+) \\ L(T^+) \end{bmatrix} = \begin{bmatrix} 0 & 0 \\ mH\ell \sinh(\ell T) & \cosh(\ell T) \end{bmatrix} \begin{bmatrix} x_c(0^+) \\ L(0^+) \end{bmatrix} + \begin{bmatrix} 1 \\ 0 \end{bmatrix} u_{fp}(T^-). \quad (34)$$

Next, applying the feedback law (32) with L^{des} a constant results in the Poincaré map being

$$\begin{aligned} \begin{bmatrix} x_c(T^+) \\ L(T^+) \end{bmatrix} &= \begin{bmatrix} \alpha - \cosh(\ell T) & \frac{(\alpha - \cosh(\ell T)) \cosh(\ell T)}{mH\ell \sinh(\ell T)} \\ mH\ell \sinh(\ell T) & \cosh(\ell T) \end{bmatrix} \begin{bmatrix} x_c(0^+) \\ L(0^+) \end{bmatrix} \\ &+ \begin{bmatrix} \frac{1-\alpha}{mH\ell \sinh(\ell T)} \\ 0 \end{bmatrix} L^{\text{des}}. \end{aligned} \quad (35)$$

The Poincaré map has fixed point

$$\begin{bmatrix} x_c^* \\ L^* \end{bmatrix} = \begin{bmatrix} \frac{1-\cosh(\ell T)}{mH\ell \sinh(\ell T)} L^{\text{des}} \\ L^{\text{des}} \end{bmatrix} \quad (36)$$

independent of α and the eigenvalues of the Poincaré map are $(\alpha, 0)$. Hence, for all $0 \leq \alpha < 1$, the fixed point is exponentially stable and moreover, (35) is bounded-input bounded-state stable with respect to the command, L^{des} .

E. Lateral Control and Turning

From (17), the time evolution of the angular momentum about the contact point is decoupled about the x - and y -axes. Therefore, once a desired angular momentum at the end of next step is given, Lateral Control is essentially identical to Longitudinal Control and (31) can be applied equally well in the lateral direction.³ **The question becomes how to decide on $L^{x \text{ des}}(T_{k+1}^-)$** , since it cannot be simply set to zero for walking with a non-zero stance width.

For walking in place or walking with zero average lateral velocity, it is sufficient to obtain $L^{x \text{ des}}$ from a periodically oscillating LIP model,

$$L^{x \text{ des}}(T_{k+1}^-) = \pm \frac{1}{2} mHW \frac{\ell \sinh(\ell T)}{1 + \cosh(\ell T)}, \quad (37)$$

where W is the desired step width. The sign is positive if next stance is left stance and negative if next stance is right stance. Lateral walking can be achieved by adding an offset to $L^{x \text{ des}}$.

To enable turning, we assume a target direction is commanded and associate a frame to it by aligning the x -axis with the target direction while keeping the z -axis vertical. To achieve turning, we then define the desired angular momentum $L^{y \text{ des}}$ and $L^{x \text{ des}}$ in the new frame and use the hip yaw-motors to align the robot in that direction.

³With a slight difference in the sign due to $L^x = -mgy_c$.

VI. PENDULUM MODELS, ZERO DYNAMICS, AND OVERALL SYSTEM STABILITY

This section establishes connections between the pendulum models of Sec. II-C and the swing phase zero dynamics as developed in [17], or more precisely, approximations of the zero dynamics. This is accomplished by analyzing how the zero dynamics are driven by the states of a bipedal robot's full-order model and its feedback controller when the closed-loop system is evolving off the zero dynamics manifold. As a main contribution, the analysis will yield conditions under which the driving terms are small and hence do not adversely affect the stability predictions associated with the exact zero dynamics. A secondary contribution of the section will be a presentation of the swing phase zero dynamics for a more general set of "virtual constraints" than those developed in [17], [23], [68].

A. Intuitive Background

An initial sense of the meaning and mathematical foundation of the swing phase zero dynamics can be gained by considering a floating-base model of a bipedal robot, and then its pinned model, that is, the model with a point or link of the robot, such as a leg end or foot, constrained to maintain a constant position respect to the ground. The given contact constraint is holonomic and constant rank, and thus using Lagrange multipliers (from the principle of virtual work), a reduced-order model compatible with the (holonomic) contact constraint is easily computed. When computing the reduced-order model, no approximations are involved, and solutions of the reduced-order model are solutions of the original floating-base model, with inputs (ground reaction forces and moments) determined by the Lagrange multiplier.

Virtual constraints are relations (i.e., constraints) on the state variables of a robot's model that are achieved through the action of actuators and feedback control instead of physical contact forces. They are called *virtual* because they can be re-programmed on the fly without modifying any physical connections among the links of the robot or its environment. We use virtual constraints to synchronize the evolution of a robot's links, so as to create exponentially stable motions. Like physical constraints, under certain regularity conditions, they induce an exact low-dimensional invariant model, called the *zero dynamics*, due to the highly influential paper [28].

Each virtual constraint imposes a relation between joint variables, and by differentiation with respect to time, a relation between joint velocities. As a consequence, for the virtual constraints studied in this paper, the dimension of the zero dynamics is the number of states in the robot's (pinned) model minus twice the number of virtual constraints (which can be at most the number of independent actuators). As explained in [69], the computation of the motor torques to impose virtual constraints parallels the Jacobian computations for the ground reaction forces in a pinned model.

B. Allowing Non-holonomic, Time-varying Virtual Constraints

In this section, we choose L as one of the states of the zero dynamics. So that fully actuated and underactuated biped

models can be addressed simultaneously, we suppose that the torque distribution matrix $B(q)$ in (1) can be split so that

$$B(q)u =: B_a(q)u_a + B_b(q)u_b, \quad (38)$$

where u_a is the torque affecting the stance ankle as in Sect. II-C and $u_b \in \mathbb{R}^n$ are actuators affecting the body coordinates, q_b . When the robot is underactuated, $B_a(q)$ is an empty column vector.

We define n virtual constraints as an output zeroing problem of the form

$$y = h(q, L, \tau) = h_0(q) - h_d(x_c, L, \tau) \quad (39)$$

where τ captures time dependence. As in Sect. II-C, we use L instead of other functions of \dot{q} because L has relative degree three with respect to all actuators except stance ankle torque, while \dot{q} has relative degree one. Hence, the relative degree of y is determined by q once u_a is fixed. Indeed, while u_b is used for imposing the virtual constraints, u_a can be used for shaping the evolution of x_c and L directly. We assume a feedback law, u_a , of the form

$$u_a = \alpha(x_c, L, \tau) \quad (40)$$

and note that u_a should respect relevant ankle torque limits and ZMP constraints when $y \equiv 0$.

Following [17], [27], [28], we make the following specific *regularity assumptions* for the virtual constraints:

A1: h is at least twice continuously differentiable and u_a is at least once differentiable.

A2: The virtual constraints (39) are designed to identically vanish on a desired nominal solution (gait) $(\bar{q}(t), \dot{\bar{q}}(t), \bar{u}(t))$ of the dynamical model (6) with $\tau(t) = t$, where the solution meets relevant constraints on motor torque, motor power, ground reaction forces, and work space. To be clear, y vanishing means

$$h_0(\bar{q}) - h_d(\bar{x}_c, \bar{L}, \tau) \equiv 0 \quad (41)$$

for $0 \leq t \leq T$, where $\bar{L}(t)$ is the angular momentum about the contact point, evaluated along the trajectory.

A3: The *decoupling matrix*

$$A(q) := \frac{\partial h(q, L, t)}{\partial q} D^{-1}(q) B_b(q) \quad (42)$$

is square and invertible along the nominal trajectory, so that, from [27] and [70], by treating u_a as a known signal, there exists a feedback controller of the form

$$u_b =: \gamma(q, \dot{q}, \tau) + \gamma_a(q, L, \tau) u_a \quad (43)$$

resulting in the closed-loop dynamics

$$\ddot{y} + K_d \dot{y} + K_p y = 0, \quad (44)$$

with $K_d > 0$ and $K_p > 0$ positive definite.

A4: The function

$$\begin{bmatrix} y \\ \dot{y} \\ x_c \\ L \end{bmatrix} \quad (45)$$

is full rank and injective in an open neighborhood of the nominal solution $(\bar{q}(t), \dot{\bar{q}}(t)) \forall t$.

From [17], [27], [28], the above assumptions imply that (y, \dot{y}, x_c, L) is a valid set of coordinates for the full-order swing phase model (2). In particular,

1) there exists an invertible differentiable function Φ such that

$$\begin{bmatrix} q \\ \dot{q} \\ \tau \end{bmatrix} = \Phi(y, \dot{y}, x_c, L, \tau), \quad \text{and} \quad (46)$$

2) the swing phase zero dynamics, that is, the dynamics of the robot compatible with $y \equiv 0$, exists and can be parameterized by (x_c, L) .

C. Zero Dynamics and Approximate Zero Dynamics

From Assumptions A1-A4, it follows that the swing phase zero dynamics exists and for $\xi = (x_c, L, \tau)$ can be expressed as

$$\dot{\xi} = f_{\text{zero}}(\xi), \quad (47)$$

when $y \equiv 0$. As with the popular pendulum models, the dimension of (47) is low, it has two states plus time. Different that the pendulum models, (47) is exact. Moreover, tools are known for relating periodic orbits of the hybrid version of (47) to corresponding orbits in the full-order model (6), including their stability properties; see Sect. VI-D.

On the basis of (10) evaluated at (46), the zero dynamics (47) can be written more explicitly as

$$\begin{aligned} \dot{x}_c &= \frac{L}{mz_c(x_c, L, \tau)} + \frac{\dot{z}_c(x_c, L, \tau)}{z_c(x_c, L, \tau)} x_c - \frac{L_c(x_c, L, \tau)}{mz_c(x_c, L, \tau)} \\ \dot{L} &= mgx_c + u_a(x_c, L, \tau) \\ \dot{\tau} &= 1. \end{aligned} \quad (48)$$

The state $\dot{\tau} = 1$ is included in (48) because, at hybrid transitions, τ is reset to zero, that is, $\tau^+ := 0$. As discussed above, this reduced-order model is exact along all trajectories of the full-order model for which $y \equiv 0$.

If one of the virtual constraints in (39) is $z_c - H$, that is, the center of mass height is regulated to a constant, then the zero dynamics (exactly) simplifies to

$$\begin{aligned} \dot{x}_c &= \frac{L}{mH} - \frac{L_c(x_c, L, \tau)}{mH} \\ \dot{L} &= mgx_c + u_a(x_c, L, \tau) \\ \dot{\tau} &= 1. \end{aligned} \quad (49)$$

This model is nonlinear and time-varying through L_c and possibly, the feedback control policy chosen for the stance ankle torque, u_a . We've argued in Sec. IV that L_c can be dropped from the model. Doing so results in the ALIP model, (20). Hence, the ALIP model is an *approximate swing phase zero dynamics* when the center of mass height is controlled to a constant.

D. Consequences for Closed-loop Stability of the Full-order Model

When the foot placement policy (32) is applied to (49) with the rest map (25), the resulting closed-loop system is a (small) perturbation of a hybrid system that possesses a family of

exponentially stable periodic orbits parameterized by L^{des} . If the virtual constraints in (39) are hybrid⁴ invariant for constant L^{des} [17], [73], [74], then

- (49) with impact map (25) is the hybrid zero dynamics, and
- an exponentially stable periodic solution of the hybrid zero dynamics is also an exponentially stable solution of the full order closed-loop system for appropriate choices of the feedback gains K_p and K_d in (44).

Consequently, the closed-loop system would possess a family of exponentially stable periodic orbits parameterized by L^{des} . If the virtual constraints are not hybrid invariant, then (49) with (25) does not form a hybrid zero dynamics in the sense of [17], but rather a *limit restriction dynamics* [75, pp. 102]. Moreover, via the Brouwer Fixed Point Theorem, reference [75, Theorem 6, pp. 105] shows each exponentially stable periodic solution of the limit restriction dynamics corresponds to an exponentially stable periodic solution of the full model for appropriate design of the feedback gains in (44).

To illustrate the correspondence between exponentially stable motions of the ALIP and the full-order model, we turn to the Rabbit model controlled via virtual constraints that implement the foot placement control law (32), the center of mass at a constant height, the torso upright, and adequate foot clearance. We then numerically estimate the Jacobian of the Poincaré map for the closed-loop full-order model and compare its dominant eigenvalues to the dominant eigenvalue of the closed-loop ALIP model; see (35).

In Table II, for various values of α in the step placement feedback controller, we show the dominant eigenvalue from the ALIP model and the dominant eigenvalue from the numerically estimated Poincaré map. We see that the dominant eigenvalue of the full-order closed-loop system corresponds to the dominant eigenvalue of the ALIP model for $0 \leq \alpha \leq 0.9$. The remaining eigenvalues of the full model are (very) small due to the gains chosen in (44). In fact, the zero dynamics captures the “weakly actuated”, slow part of the full-order model that is evolving under the influence of gravity.

α	ALIP	Rabbit
0.9	0.81	0.781
0.8	0.64	0.601
0.7	0.49	0.442
0.6	0.36	0.299
0.5	0.25	0.168
0.4	0.16	0.052
0.3	0.09	0.013
0.2	0.04	2e-4
0.1	0.01	2e-4
0.0	0.00	1e-4

TABLE II: Largest eigenvalues of ALIP and Rabbit under different α , for a two-step Poincaré map. Because the Poincaré map is computed over two steps, the ALIP’s largest eigenvalue is α^2 .

⁴Hybrid invariance means that if y and \dot{y} are zero before the impact, they will also be zero after the impact. References [71], [72] show how to systematically modify a given set of virtual constraints to achieve hybrid invariance.

Remark: We numerically obtained the Jacobian of the Poincaré map for Rabbit with the foot placement controller by the method symmetric differences; δ deviations were applied on ten states (Rabbit has 5 degree of freedom) and we measured the corresponding responses after two steps. The δ was chosen from the set $\{\pm 0.05, \pm 0.1, \pm 0.2, \pm 0.3\}$; see Table III.

α	ALIP	$\delta = \pm 0.05$	$\delta = \pm 0.1$	$\delta = \pm 0.2$	$\delta = \pm 0.3$
0.9	0.81	0.780	0.783	0.781	0.779
0.8	0.64	0.602	0.602	0.601	0.599
0.7	0.49	0.442	0.443	0.441	0.439
0.6	0.36	0.299	0.301	0.300	0.299
0.5	0.25	0.170	0.170	0.168	0.164
0.4	0.16	0.054	0.053	0.052	0.051
0.3	0.09	0.014	0.014	0.012	0.011

TABLE III: Numerical support for estimating the Jacobian of the two-step Poincaré map. The dominant eigenvalue of Rabbit model is insensitive to the perturbation used in estimating the Jacobian.

E. Non-periodic Walking

The desired angular momentum, L^{des} , determines the fixed point of the Poincaré map and hence the walking speed of the robot. While varying L^{des} causes the walking speed to change, the analysis of the controller has only been presented for a constant value of L^{des} . Reference [76] analyzes gait transitions in the formalism of the hybrid zero dynamics when L^{des} is switched “infrequently”, meaning the closed-loop system is moving from a neighborhood of one periodic orbit to another. References [77], [78] generalize tools from Input-to-State Stability (ISS) of ODEs to the case of hybrid models. These results apply to time-varying L^{des} . The experimental work reported in Sec. IX includes examples of rapidly varying L^{des} , turn direction, and ground height.

F. Varying Center of Mass Height

We have seen that the difference between the zero dynamics of a real robot and a pendulum model is the term related to L_c . In previous sections, we have shown that the L_c term has very little effect on the L dynamics when z_c is constant. This observation can be extended to the case when z_c is not constant but virtually constrained by (x_c, L, τ) .

In Fig. 12, we illustrate that when the z_c is a function of time, the pendulum dynamics can still be used to predict accurately the zero dynamics of Rabbit.

VII. INTEGRATING VIRTUAL CONSTRAINTS AND ANGULAR-MOMENTUM-BASED FOOT PLACEMENT

In this section we generate virtual constraints for a 3D robot such as Cassie. As in [79], we leave the stance toe passive.

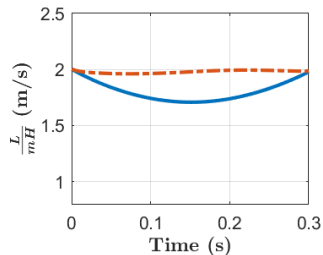


Fig. 12: Trajectory of L and its prediction in a simulation of Rabbit. The instantaneous values are shown in **blue** and the predicted value at the end of the step is shown in **red**. In the prediction of L , the virtual constraint on center of mass height for the model model and for Rabbit are set to $z_c = 0.6 + 0.05 \sin(\frac{T}{2\pi}\tau - \frac{\pi}{2}) + 0.05$, where T is the step time. Large z_c oscillations often occur in running. Here, we modify the ground model to pin the stance foot to the ground, so that we can impose a non-trivial z_c oscillation in periodic walking.

Consequently, there are nine (9) control variables, listed below from the top of the robot to the end of the swing leg,

$$h_0 = \begin{bmatrix} \text{torso pitch} \\ \text{torso roll} \\ \text{stance hip yaw} \\ \text{swing hip yaw} \\ p_{st \rightarrow CoM}^z \\ p_{sw \rightarrow CoM}^x \\ p_{sw \rightarrow CoM}^y \\ p_{sw \rightarrow CoM}^z \\ \text{swing toe absolute pitch} \end{bmatrix}. \quad (50)$$

For later use, we denote the value of h_0 at the beginning of the current step by $h_0(T_{k-1}^+)$. When referring to individual components, we'll use $h_{03}(T_{k-1}^+)$, for example.

We first discuss variables that are constant. The reference values for torso pitch, torso roll, and swing toe absolute pitch are constant and zero, while the reference for $p_{st \rightarrow CoM}^z$, which sets the height of the CoM with respect to the ground, is constant and equal to H .

We next introduce a phase variable

$$s := \frac{t - T_{k-1}^+}{T} \quad (51)$$

that will be used to define quantities that vary throughout the step to create “leg pumping” and “leg swinging”. The reference trajectories of $p_{sw \rightarrow CoM}^x$ and $p_{sw \rightarrow CoM}^y$ are defined such that:

- at the beginning of a step, their reference value is their actual position;
- the reference value at the end of the step implements the foot placement strategy in (31); and
- in between a half-period cosine curve is used to connect them, which is similar to the trajectory of an ordinary (non-inverted) pendulum.

The reference trajectory of $p_{sw \rightarrow CoM}^z$ assumes the ground is flat and the control is perfect:

- at mid stance, the height of the foot above the ground is given by z_{CL} , for the desired vertical clearance.

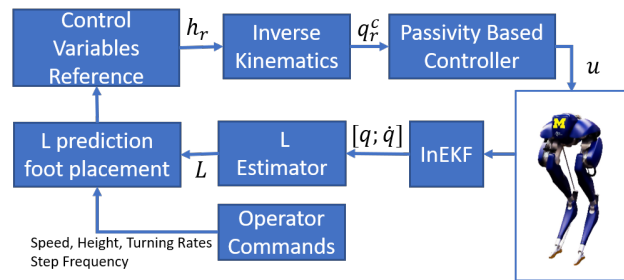


Fig. 13: Block diagram of the implemented controller.

The reference trajectories for the stance hip and swing hip yaw angles are simple straight lines connecting their initial actual position and their desired final positions. For walking in a straight line, the desired final position is zero. To include turning, the final value has to be adjusted. Suppose that a turn angle of ΔD_k^{des} radians is desired. One half of this value is given to each yaw joint:

- $+\frac{1}{2}\Delta D_k^{\text{des}} \rightarrow$ swing hip yaw; and
- $-\frac{1}{2}\Delta D_k^{\text{des}} \rightarrow$ stance hip yaw

The signs may vary with the convention used on other robots.

The final result for Cassie Blue is

$$h_d(s) := \begin{bmatrix} 0 \\ 0 \\ (1-s)h_{03}(T_{k-1}^+) + s(-\frac{1}{2}(\Delta D_k)) \\ (1-s)h_{04}(T_{k-1}^+) + s(\frac{1}{2}(\Delta D_k)) \\ H \\ \frac{1}{2}[(1 + \cos(\pi s))h_{06}(T_{k-1}^+) + (1 - \cos(\pi s))p_{sw \rightarrow CoM}^x \text{ des}(T_k^-)] \\ \frac{1}{2}[(1 + \cos(\pi s))h_{07}(T_{k-1}^+) + (1 - \cos(\pi s))p_{sw \rightarrow CoM}^y \text{ des}(T_k^-)] \\ 4z_{cl}(s - 0.5)^2 + (H - z_{CL}); \\ 0 \end{bmatrix}. \quad (52)$$

When implemented with an Input-Output Linearizing Controller⁵ so that h_0 tracks h_d , the above control policy allows Cassie to move in 3D in simulation.

VIII. PRACTICAL IMPLEMENTATION ON CASSIE

This section resolves several issues that prevent the basic controller from being implemented on Cassie Blue.

A. IMU and EKF

In a real robot, an IMU and an EKF are needed to estimate the linear position and rotation matrix at a fixed point on the robot, along with their derivatives. Cassie uses a VectorNav IMU. We used the Contact-aided Invariant EKF developed in [81], [82] to estimate the torso velocity. With these signals in hand, we could estimate angular momentum about the contact point.

B. Filter for Angular Momentum

Angular Momentum about the contact toe could be computed directly from estimated $[q, \dot{q}]$, but it is noisy. We used a Kalman Filter to improve the estimation. The models we used are

⁵The required kinematic and dynamics functions are generated with FROST [80].

$$\text{Prediction: } L^y(k) = AL^y(k-1) + Bu(k) + \delta \quad (53)$$

$$\text{Correction: } L^y_{\text{obs}}(k) = CL^y(k) + \epsilon$$

where $A = B = C = 1$, $u(k) = (mgx_c(k) + u_a(k))\Delta T$. The update formula for angular momentum is

$$L^y(k) = (I - K(k)C)(AL^y(k-1) + Bu(k)) + K(k)L^y_{\text{obs}}(k) \quad (54)$$

The Kalman Gain $K(k)$ is obtained following the algorithm described in [83, Sec 3.2].

C. Inverse Kinematics

Input-Output Linearization does not work well in experiments [79], [84], [85]. To use a passivity-based controller for tracking that is inspired by [70], we need to convert the reference trajectories for the variables in (50) to reference trajectories for Cassie’s actuated joints,

$$q^{\text{act}} = \begin{bmatrix} \text{torso pitch} \\ \text{torso roll} \\ \text{stance hip yaw} \\ \text{swing hip yaw} \\ \text{stance knee pitch} \\ \text{swing hip roll} \\ \text{swing hip pitch} \\ \text{swing knee pitch} \\ \text{swing toe pitch} \end{bmatrix}. \quad (55)$$

Iterative inverse kinematics is used to convert the controlled variables in (50) to the actuated joints.

D. Passivity-based Controller

We adapt the passivity-based controller developed in [70] to achieve joint-level tracking. This method takes the full-order model of robot into consideration and, on a perfect model, will drive the virtual constraints asymptotically to zero. The derivation is given in the Appendix.

E. Springs

On the swing leg, the spring deflection is small and thus we are able to assume the leg to be rigid. On the stance leg, the spring deflection is non-negligible and hence requires compensation. While there are encoders on both sides of the spring to measure its deflection, direct use of this leads to oscillations. The deflection of the spring is instead estimated through a simplified model.

F. COM Velocity in the Vertical Direction

When Cassie’s walking speed exceeds one meter per second, the assumption that $v_{\text{CoM}}^z \approx 0$ breaks down due to spring and imperfect low level control, and (29) is no longer valid. Hence, we use

$$L^y(T_k^+) = L^y(T_k^-) + mv_{\text{CoM}}^z(T_k^-)(p_{\text{sw} \rightarrow \text{CoM}}^x(T_k^-) - p_{\text{st} \rightarrow \text{CoM}}^x(T_k^-)). \quad (56)$$

From this, the foot placement is updated to

$$p_{\text{sw} \rightarrow \text{CoM}}^x \text{ des}(T_k^-) = \frac{L^y \text{ des}(T_{k+1}^-)}{m(H\ell \sinh(\ell T) - v_{\text{CoM}}^z \cosh(\ell T))} - \frac{(L^y(T_k^-) + mv_{\text{CoM}}^z(T_k^-)p_{\text{st} \rightarrow \text{CoM}}^x(T_k^-)) \cosh(\ell T)}{m(H\ell \sinh(\ell T) - v_{\text{CoM}}^z \cosh(\ell T))}. \quad (57)$$

Remark: In our experiments v_{CoM}^z becomes negative at the end of a step when the robot is walking fast. If we still use (31) to decide foot placement, which is based on the reset map (29), in the lateral direction $L^x(T_k^+)$ will be overestimated. This in turn leads to the lateral foot placement being commanded further from the body than it should be. At the end of the next step, the magnitude of L^x will be larger than expected, requires even further lateral foot placement from the body. The final phenomenon is abnormally large step width.

IX. EXPERIMENTAL RESULTS

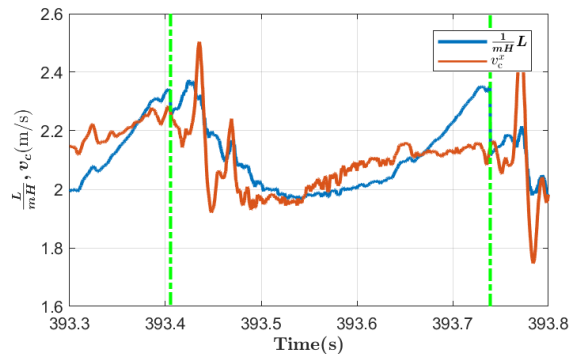
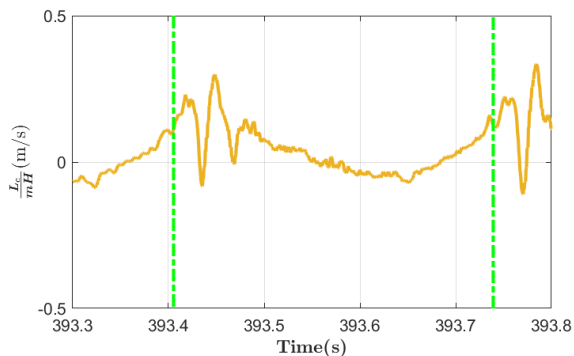
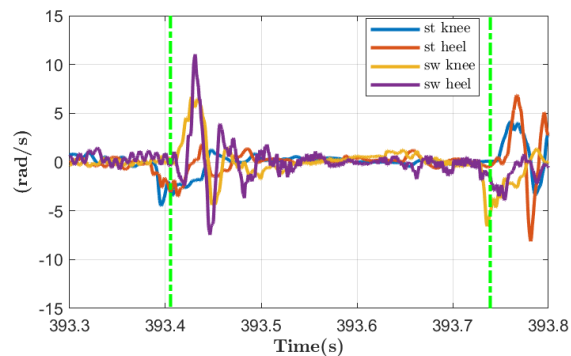
The controller was implemented on Cassie Blue. The closed-loop system consisting of robot and controller was evaluated in a number of situations that are itemized below.

- **Walking in a straight line on flat ground.** Cassie could walk in place and walk stably for speeds ranging from zero to 2.1 m/s.
- **Diagonal Walking.** Cassie is able to walk simultaneously forward and sideways on grass, at roughly 1 m/s in each direction.
- **Sharp turn.** While walking at roughly 1 m/s, Cassie Blue effected a 90° turn in six steps, without slowing down.
- **Rejecting the classical kick to the base of the hips.** Cassie was able to remain upright under “moderate” kicks in the longitudinal direction. The disturbance rejection in the lateral direction is not as robust as the longitudinal, which is mainly caused by Cassie’s physical design: small hip roll motor position limits.
- **Finally we address walking on rough ground.** Cassie Blue was tested on the iconic Wave Field of the University of Michigan North Campus. The foot clearance was increased from 10 cm to 20 cm to handle the highly undulating terrain. Cassie is able to walk through the “valley” between the large humps with ease at a walking pace of roughly 0.75 m/s, without falling in all tests. The row of ridges running east to west in the Wave Field are roughly 60 cm high, with a sinusoidal structure. We estimate the maximum slope to be 40 degrees. Cassie is able to cross several of the large humps in a row, but also fell multiple times. On a more gentle, straight grassy slope of roughly 22 degrees near the laboratory, Cassie can walk up it with no difficulty with 20cm foot clearance.

The experimental data is analyzed in Fig. 14 and 15. The figures support the advantages of using L to indicate robot status and the accuracy of ALIP model, as discussed in Sec III and IV.

X. CONCLUSIONS

We established connections between various approximate pendulum models that are commonly used for heuristic controller design and those that are more common in the feedback

(a) L and v_c (b) L_c 

(c) Spring deflection rates for stance and swing legs

Fig. 14: Experimental data from Cassie walking forward at about 2m/s. To ensure a fair comparison, L is not smoothed by Kalman Filter described in VIII-B. L , v_c and L_c are computed from the same states $[q, \dot{q}]$. v_c^x and L_c oscillates at the beginning of a step because of their relative degree one nature, in particular, they are heavily affected by the spring oscillation just after impact. L is mostly smooth because it has relative degree three, except near impact when the robot is in double support phase and L has relative degree one. The sudden jump in L at impact is caused by nonzero v_c^z . The smoothness difference shows another advantage of L : it can be used in feedback control without being heavily filtered.

control literature where formal stability guarantees are the norm. The paper clarified commonalities and differences in the two perspectives for using low-dimensional models. In the process of doing so, we argued that models based on

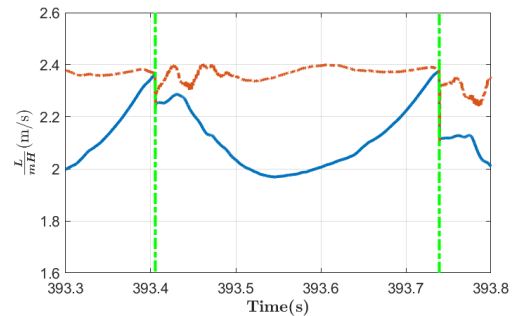


Fig. 15: Prediction made in experiment from Cassie walking forward at about 2m/s. The instantaneous values are shown in blue and the predicted value at the end of the step is shown in red. The Kalman Filter described in VIII-B has been applied.



(a) Fast Walking

(b) Rough Terrain



(c) Disturbance Rejection



(d) A Fast 90 Degree Turn with a Long Stride

Fig. 16: Images from several closed-loop experiments conducted with Cassie Blue and the controller developed in this paper. A short video compilation of these experiments is available in [86]. Longer versions can be found in [87].

angular momentum about the contact point provide more accurate representations of robot state than models based on linear velocity. Specifically, we showed that an approximate (pendulum or zero dynamics) model parameterized by angular momentum provides better predictions for foot placement on

a physical robot (e.g., legs with mass) than does a related approximate model parameterized in terms of linear velocity. While ankle torque, if available, can achieve small changes in angular momentum during a step, the limitations of foot roll prevent ankle torque from achieving large changes in angular momentum during a step. For this reason, we focused our analysis on regulating angular momentum about the contact point step-to-step and not within a step. We implemented a one-step-ahead angular-momentum-based controller on Cassie, a 3D robot, and demonstrated high agility and robustness in experiments. Using our new controller, Cassie was able to accomplish a wide range of tasks with nothing more than common sense task-based tuning: a higher step frequency to walk at 2.1 m/s and extra foot clearance to walk over slopes exceeding 22 degrees. Moreover, in the current implementation, there is no optimization of trajectories used in the implementation on Cassie. The robot's performance is currently limited by the hand-designed trajectories leading to joint-limit violations and foot slippage. These limitations will be mitigated by incorporating optimization and or constraints via MPC.

In addition to the foot placement scheme described in this paper, the ALIP model can be combined with many other control methods that have been implemented on the LIP model: it can be used with ZMP in an MPC scheme as in [11]–[13], or used with Capture Point as in [4], [5], or used with an estimated L_c [15], [16]. As has already been done in [37], L can be regulated by controlling the center of mass velocity just before impact, as well.

APPENDIX

A. Constant Pendulum Length

Suppose that one component of the virtual constraints in (39) is $r_c(q) - R$, where R is a constant. Then $y \equiv 0$ yields $r_c = R$, simplifying (12) to

$$\begin{aligned} \dot{\theta}_c &= \frac{L - L_c}{mR^2} \\ \dot{L} &= mgR \sin(\theta_c) + u_a. \end{aligned} \quad (58)$$

At this point, no approximations have been made and the models is valid everywhere that $r_c(q) \equiv R$. An interesting aspect of this pendulum model is that it does not depend on \dot{R} , and thus imperfections in achieving the virtual constraint $r_c = R$ have a smaller effect here than in (17), where \dot{z} would appear when $z_c \neq H$, or in (16), where both \dot{z}_c and \ddot{z}_c would appear.

As with (17), the model (58) is driven by the strongly actuated states q_b, \dot{q}_b through L_c and the same discussion applies. Dropping L_c in (10) results in

$$\begin{aligned} \dot{\theta}_c &= \frac{L}{mR^2} \\ \dot{L} &= mgR \sin(\theta_c) + u_a, \end{aligned} \quad (59)$$

which is nonlinear in θ_c . However, for $R = 1$ and a step length of 60 cm, $\max \theta_c \approx \pi/6$, and for 70 cm, $\max \theta_c \approx \pi/4$, giving

simple bounds on the approximation error,

$$\begin{aligned} \frac{1}{\pi/6} \int_0^{\pi/6} (\theta - \sin(\theta)) d\theta &< 0.006 \\ \frac{1}{\pi/4} \int_0^{\pi/4} (\theta - \sin(\theta)) d\theta &< 0.02. \end{aligned}$$

Moreover, if desired, one can chose K to set

$$\frac{1}{\theta_{\max}} \left| \int_0^{\theta_{\max}} (K\theta - \sin(\theta)) d\theta \right| = 0.$$

For $\theta_{\max} = \pi/4$, the value is $K \approx 0.95$. While a linear approximation is useful for having a closed-form solution, numerically integrating the nonlinear model (59) in real time is certainly feasible.

The discussion on the approximate zero dynamics can be repeated here. The associated impact map is nonlinear and can be linearized about a nominal solution.

B. Passivity-based Input-Output Stabilization

The material presented here adapts the original work in [70] to a floating-base model

$$D(q)\ddot{q} + H(q, \dot{q}) = Bu + J_s^\top \tau_s + J_g(q)^\top \tau_g, \quad (60)$$

with u the vector of motor torques, τ_s the spring torques, and τ_g is the contact wrench. During the single support phase, the blade-shape foot on Cassie provides five holonomic constraints, leaving only foot roll free. To simplify the problem, we also assume the springs are rigid, adding two constraint on each leg. These constraints leave the original 20-degree-of-freedom floating base model with 11 degrees of freedom.

The constraints mentioned above can be written as

$$\begin{cases} J_s \ddot{q} = 0 \\ J_g(q) \ddot{q} + \dot{J}_g(q) \dot{q} = 0. \end{cases} \quad (61)$$

Combining (60) and (61) yields the full model for Cassie in single support,

$$\underbrace{\begin{bmatrix} D & -J_s^\top & -J_g^\top \\ J_s & 0 & 0 \\ J_g & 0 & 0 \end{bmatrix}}_{\bar{D}} \underbrace{\begin{bmatrix} \ddot{q} \\ \tau_s \\ \tau_g \end{bmatrix}}_f + \underbrace{\begin{bmatrix} H \\ 0 \\ \dot{J}_g \dot{q} \end{bmatrix}}_{\bar{H}} = \underbrace{\begin{bmatrix} B \\ 0 \\ 0 \end{bmatrix}}_{\bar{B}} u \quad (62)$$

For simplicity we assume that the components of q have already been ordered such that $q = [q_c, q_u]^\top$, where q_c are the coordinates chosen to be controlled and q_u are the free coordinates. Define $\lambda = [q_u, \tau_s, \tau_g]^\top$ and partition (62) as

$$\begin{cases} \tilde{D}_{11} \ddot{q}_c + \tilde{D}_{12} \lambda + \tilde{H}_1 = \tilde{B}_1 u \\ \tilde{D}_{21} \ddot{q}_c + \tilde{D}_{22} \lambda + \tilde{H}_2 = \tilde{B}_2 u \end{cases} \quad (63)$$

The vector λ can be eliminated from these equations, resulting in

$$\bar{D} \ddot{q}_c + \bar{H} = \bar{B} u, \quad (64)$$

where

$$\begin{aligned} \bar{D} &= \tilde{D}_{11} - \tilde{D}_{12} \tilde{D}_{22}^{-1} \tilde{D}_{21} \\ \bar{H} &= \tilde{H}_1 - \tilde{D}_{12} \tilde{D}_{22}^{-1} \tilde{H}_2 \\ \bar{B} &= \tilde{B}_1 - \tilde{D}_{12} \tilde{D}_{22}^{-1} \tilde{B}_2. \end{aligned}$$

We note that \tilde{D}_{22} being invertible and \bar{D} being positive definite both follow from \bar{D} being positive definite. Later, we need \bar{B} to be invertible; *this is an assumption* similar to that in (42). Equation (64) is what we will focus on from here on.

For the Passivity-based Controller, the error dynamic for $y := q_c - q_r$ and is designed to be [88]

$$\bar{D}\ddot{y} + (\bar{C} + k_d)\dot{y} + k_p y = 0, \quad (65)$$

where \bar{C} is the Coriolis/centrifugal matrix in \bar{H} and it is chosen such that $\bar{D} = \bar{C} + \bar{C}^\top$. From (64) and (65), we have

$$u = \bar{B}^{-1}(\bar{D}\ddot{q}_r + \bar{H}) - \bar{B}^{-1}(k_p y + (\bar{C} + k_d)\dot{y}). \quad (66)$$

Compared with a standard Input-Output Linearization controller, whose error dynamics and command torque are

$$\dot{y} + k_d \dot{y} + k_p y = 0, \quad \text{and} \quad (67)$$

$$u = \bar{B}^{-1}(\bar{D}\ddot{q}_r + \bar{H}) - \bar{B}^{-1}\bar{D}(k_p y + k_d \dot{y}), \quad (68)$$

the passivity-based controller induces less cancellation of the robot's dynamics, and if k_p and k_d are chosen to be diagonal matrices, the tracking errors are approximately decoupled because, for Cassie, \bar{B}^{-1} is close to diagonal. This controller provides improved tracking performance over the straight-up PD implementation in [79].

ACKNOWLEDGMENT

Toyota Research Institute provided funds to support this work. Funding for J. Grizzle was in part provided by NSF Award No. 1808051. The authors thank Omar Harib and Jiunn-Kai Huang for their assistance in the experiments.

REFERENCES

- [1] H. Miura and I. Shimoyama. Dynamic walk of a biped. *International Journal of Robotics Research*, 3(2):60–74, 1984.
- [2] Shuuji Kajita, Fumio Kanehiro, Kenji Kaneko, Kazuhito Yokoi, and Hirohisa Hirukawa. The 3d linear inverted pendulum mode: A simple modeling for a biped walking pattern generation. In *Proceedings 2001 IEEE/RSJ International Conference on Intelligent Robots and Systems. Expanding the Societal Role of Robotics in the Next Millennium (Cat. No. 01CH37180)*, volume 1, pages 239–246. IEEE, 2001.
- [3] R. Blickhan. The spring-mass model for running and hopping. *Journal of Biomechanics*, 22(11-12):1217–1227, 1989.
- [4] Jerry Pratt, John Carff, Sergey Drakunov, and Ambarish Goswami. Capture point: A step toward humanoid push recovery. In *2006 6th IEEE-RAS international conference on humanoid robots*, pages 200–207. IEEE, 2006.
- [5] Johannes Engelsberger, Christian Ott, Máximo A Roa, Alin Albu-Schäffer, and Gerhard Hirzinger. Bipedal walking control based on capture point dynamics. In *2011 IEEE/RSJ International Conference on Intelligent Robots and Systems*, pages 4420–4427. IEEE, 2011.
- [6] Ting Wang and Christine Chevallereau. Stability analysis and time-varying walking control for an under-actuated planar biped robot. *Robotics and Autonomous Systems*, 59(6):444 – 456, 2011.
- [7] Xiaobin Xiong and Aaron D Ames. Orbit characterization, stabilization and composition on 3d underactuated bipedal walking via hybrid passive linear inverted pendulum model. In *2019 IEEE/RSJ International Conference on Intelligent Robots and Systems (IROS)*, pages 4644–4651. IEEE, 2019.
- [8] Agility Robotics. Robots. <https://www.agilityrobotics.com/robots#cassie>, 2021.
- [9] A. Goswami and V. Kalle. Rate of change of angular momentum and balance maintenance of biped robots. In *Proc. of the 2004 IEEE International Conference on Robotics and Automation, New Orleans, LA*, volume 4, pages 3785–90, 2004.
- [10] M. Popovic, A. Hofmann, and H. Herr. Zero spin angular momentum control: definition and applicability. In *4th IEEE/RAS International Conference on Humanoid Robots, 2004.*, volume 1, pages 478–493 Vol. 1, 2004.
- [11] S. Kajita, F. Kanehiro, K. Kaneko, K. Fujiwara, K. Harada, K. Yokoi, and H. Hirukawa. Biped walking pattern generation by using preview control of zero-moment point. In *ICRA'03*, 2003.
- [12] Koichi Nishiwaki and Satoshi Kagami. High frequency walking pattern generation based on preview control of zmp. In *Proceedings 2006 IEEE International Conference on Robotics and Automation, 2006. ICRA 2006.*, pages 2667–2672. IEEE, 2006.
- [13] Pierre-Brice Wieber. Trajectory free linear model predictive control for stable walking in the presence of strong perturbations. In *2006 6th IEEE-RAS International Conference on Humanoid Robots*, pages 137–142. IEEE, 2006.
- [14] Johannes Engelsberger and Christian Ott. Integration of vertical com motion and angular momentum in an extended capture point tracking controller for bipedal walking. In *2012 12th IEEE-RAS International Conference on Humanoid Robots (Humanoids 2012)*, pages 183–189. IEEE, 2012.
- [15] Tim Seyde, Apoorv Shrivastava, Johannes Engelsberger, Sylvain Bertrand, Jerry Pratt, and Robert J Griffin. Inclusion of angular momentum during planning for capture point based walking. In *2018 IEEE International Conference on Robotics and Automation (ICRA)*, pages 1791–1798. IEEE, 2018.
- [16] Sung-Hee Lee and Ambarish Goswami. Reaction mass pendulum (rmp): An explicit model for centroidal angular momentum of humanoid robots. In *Proceedings 2007 IEEE International Conference on Robotics and Automation*, pages 4667–4672. IEEE, 2007.
- [17] E. R. Westervelt, J. W. Grizzle, C. Chevallereau, J. H. Choi, and B. Morris. *Feedback Control of Dynamic Bipedal Robot Locomotion*. Control and Automation. CRC Press, Boca Raton, FL, June 2007.
- [18] T. Yang, E. R. Westervelt, A. Serrani, and J. P. Schmiedeler. A framework for the control of stable aperiodic walking in underactuated planar bipeds. *Autonomous Robots*, 27(3):277–290, 2009.
- [19] Anne E. Martin, David C. Post, and James P. Schmiedeler. Design and experimental implementation of a hybrid zero dynamics-based controller for planar bipeds with curved feet. *The International Journal of Robotics Research*, 33(7):988–1005, 2014.
- [20] H. Zhao, J. Horn, J. Reher, V. Paredes, and A. D. Ames. A hybrid systems and optimization-based control approach to realizing multi-contact locomotion on transfemoral prostheses. In *IEEE Conference on Decision and Control (CDC)*, pages 1607–1612, Dec 2015.
- [21] Jacob Reher, Eric A Cousineau, Ayonga Hereid, Christian M Hubicki, and Aaron D Ames. Realizing dynamic and efficient bipedal locomotion on the humanoid robot durus. In *2016 IEEE International Conference on Robotics and Automation (ICRA)*, pages 1794–1801. IEEE, 2016.
- [22] J. Reher, E. A. Cousineau, A. Hereid, C. M. Hubicki, and A. D. Ames. Realizing dynamic and efficient bipedal locomotion on the humanoid robot DURUS. In *2016 IEEE International Conference on Robotics and Automation (ICRA)*, pages 1794–1801, May 2016.
- [23] Brent Griffin and Jessy Grizzle. Nonholonomic virtual constraints for dynamic walking. In *2015 54th IEEE Conference on Decision and Control (CDC)*, pages 4053–4060. IEEE, 2015.
- [24] Ayush Agrawal, Omar Harib, Ayonga Hereid, Sylvain Finet, Matthieu Masselin, Laurent Praly, Aaron D. Ames, Koushil Sreenath, and Jessy W. Grizzle. First steps towards translating HZD control of bipedal robots to decentralized control of exoskeletons. *IEEE Access*, 5:9919–9934, 2017.
- [25] Thomas Gurriet, Sylvain Finet, Guilhem Boeris, Alexis Duburcq, Ayonga Hereid, Omar Harib, Matthieu Masselin, Jessy Grizzle, and Aaron D Ames. Towards restoring locomotion for paraplegics: Realizing dynamically stable walking on exoskeletons. In *C-ICRA*, pages 2804–2811. IEEE, 2018.
- [26] Xingye Da and Jessy Grizzle. Combining trajectory optimization, supervised machine learning, and model structure for mitigating the curse of dimensionality in the control of bipedal robots. *The International Journal of Robotics Research*, 38(9):1063–1097, 2019.
- [27] A. Isidori. *Nonlinear Control Systems*. Springer-Verlag, Berlin, third edition, 1995.
- [28] C. Byrnes and A. Isidori. Asymptotic stabilization of nonlinear minimum phase systems. *IEEE Transactions on Automatic Control*, 37(6):1122–37, 1991.
- [29] E. R. Westervelt and J. W. Grizzle. Design of asymptotically stable walking for a 5-link planar biped walker via optimization. In *Proc. of the 2002 IEEE International Conference on Robotics and Automation, Washington, D.C.*, pages 3117–22, 2002.
- [30] Ioannis Poulakakis and Jessy W Grizzle. The spring loaded inverted pendulum as the hybrid zero dynamics of an asymmetric hopper. *IEEE Transactions on Automatic Control*, 54(8):1779–1793, 2009.

- [31] Ayonga Hereid, Shishir Kolathaya, Mikhail S. Jones, Johnathan Van Why, Jonathan W. Hurst, and Aaron D. Ames. Dynamic multi-domain bipedal walking with ATRIAS through SLIP based human-inspired control. In *Proceedings of the 17th International Conference on Hybrid Systems: Computation and Control, HSCC '14*, pages 263–272, New York, NY, USA, 2014. ACM.
- [32] Yu-Ming Chen and Michael Posa. Optimal reduced-order modeling of bipedal locomotion. In *2020 IEEE International Conference on Robotics and Automation (ICRA)*, pages 8753–8760. IEEE, 2020.
- [33] A. Sano and J. Furusho. Realization of natural dynamic walking using the angular momentum information. In *Proc. of the 1990 IEEE International Conference on Robotics and Automation, Cincinnati, OH*, pages 1476–81, 1990.
- [34] E. Westervelt, J. W. Grizzle, and D.E. Koditschek. Hybrid zero dynamics of planar biped walkers. *IEEE Transactions on Automatic Control*, 48(1):42–56, January 2003.
- [35] JW Grizzle, Claude H Moog, and Christine Chevallereau. Nonlinear control of mechanical systems with an unactuated cyclic variable. *IEEE Transactions on Automatic Control*, 50(5):559–576, 2005.
- [36] Morteza Azad and Roy Featherstone. Angular momentum based controller for balancing an inverted double pendulum. In *Romansy 19—Robot Design, Dynamics and Control*, pages 251–258. Springer, 2013.
- [37] Matthew J Powell and Aaron D Ames. Mechanics-based control of underactuated 3d robotic walking: Dynamic gait generation under torque constraints. In *2016 IEEE/RSJ International Conference on Intelligent Robots and Systems (IROS)*, pages 555–560. IEEE, 2016.
- [38] Yukai Gong and Jessy Grizzle. One-step ahead prediction of angular momentum about the contact point for control of bipedal locomotion: Validation in a lip-inspired controller. In *2021 IEEE International Conference on Robotics and Automation (ICRA)*, pages 2832–2838. IEEE, 2021.
- [39] Brent Griffin and Jessy Grizzle. Nonholonomic virtual constraints and gait optimization for robust walking control. *The International Journal of Robotics Research*, page 0278364917708249, 2016.
- [40] Shuuji Kajita, Fumio Kanehiro, Kenji Kaneko, Kiyoshi Fujiwara, Kensuke Harada, Kazuhito Yokoi, and Hirohisa Hirukawa. Biped walking pattern generation by using preview control of zero-moment point. In *ICRA*, volume 3, pages 1620–1626, 2003.
- [41] Xiaobin Xiong, Jenna Reher, and Aaron D Ames. Global position control on underactuated bipedal robots: Step-to-step dynamics approximation for step planning. In *2021 IEEE International Conference on Robotics and Automation (ICRA)*, pages 2825–2831. IEEE, 2021.
- [42] Kaveh Akbari Hamed, Nasser Sadati, William A Gruver, and Guy A Dumont. Stabilization of periodic orbits for planar walking with noninstantaneous double-support phase. *IEEE Transactions on Systems, Man, and Cybernetics-Part A: Systems and Humans*, 42(3):685–706, 2011.
- [43] Wen-Loong Ma, Kaveh Akbari Hamed, and Aaron D Ames. First steps towards full model based motion planning and control of quadrupeds: A hybrid zero dynamics approach. In *2019 IEEE/RSJ International Conference on Intelligent Robots and Systems (IROS)*, pages 5498–5503. IEEE, 2019.
- [44] Jacob P Reher, Ayonga Hereid, Shishir Kolathaya, Christian M Hubicki, and Aaron D Ames. Algorithmic foundations of realizing multi-contact locomotion on the humanoid robot durus. *Proc. 12th Adv. Robot. Algorithmic Found. Robot.*, 13:400–415, 2020.
- [45] Takumi Kamioka, Hiroyuki Kaneko, Toru Takenaka, and Takahide Yoshiike. Simultaneous optimization of zmp and footsteps based on the analytical solution of divergent component of motion. In *2018 IEEE International Conference on Robotics and Automation (ICRA)*, pages 1763–1770, 2018.
- [46] J. H. Choi and J. W. Grizzle. Planar bipedal walking with foot rotation. In *Proceedings of the American Control Conference*, pages 4909–4916, Portland, OR, 2005.
- [47] Victor Paredes and Ayonga Hereid. Dynamic locomotion of a lower-limb exoskeleton through virtual constraints based zmp regulation. In *Dynamic Systems and Control Conference*, volume 84270, page V001T14A001. American Society of Mechanical Engineers, 2020.
- [48] C. Chevallereau, G. Abba, Y. Aoustin, F. Plestan, E. R. Westervelt, C. Canudas-de-Wit, and J. W. Grizzle. RABBIT: A testbed for advanced control theory. *IEEE Control Systems Magazine*, 23(5):57–79, October 2003.
- [49] Y. Hurmuzlu and T.H. Chang. Rigid body collisions of a special class of planar kinematic chains. *IEEE Transactions on Systems, Man, and Cybernetics*, 22(5):964–971, 1992.
- [50] Y. Hurmuzlu. Dynamics of bipedal gait - part 1: objective functions and the contact event of a planar five-link biped. *Journal of Applied Mechanics*, 60:331–336, June 1993.
- [51] J. W. Grizzle, G. Abba, and F. Plestan. Asymptotically stable walking for biped robots: Analysis via systems with impulse effects. *IEEE Transactions on Automatic Control*, 46:51–64, January 2001.
- [52] Shuuji Kajita and Kazuo Tani. Study of dynamic biped locomotion on rugged terrain-theory and basic experiment. In *Advanced Robotics, 1991. Robots in Unstructured Environments', 91 ICAR., Fifth International Conference on*, pages 741–746. IEEE, 1991.
- [53] Omar Harib, Ayonga Hereid, Ayush Agrawal, Thomas Gurriet, Sylvain Finet, Guilhem Boeris, Alexis Duburcq, M. Eva Mungai, Matthieu Masselien, Aaron D. Ames, Koushil Sreenath, and Jessy Grizzle. Feedback control of an exoskeleton for paraplegics: Toward robustly stable hands-free dynamic walking. *arXiv preprint arXiv:1802.08322 [cs.RO]*, 2018.
- [54] H-M Maus, S W Lipfert, M Gross, J Rummel, and A Seyfarth. Upright human gait did not provide a major mechanical challenge for our ancestors. *Nature Communications*, 1(6):70, January 2010.
- [55] P-B Wieber. Holonomy and nonholonomy in the dynamics of articulated motion. In *Fast motions in biomechanics and robotics*, pages 411–425. Springer, 2006.
- [56] Jerry E Pratt and Russ Tedrake. Velocity-based stability margins for fast bipedal walking. In *Fast Motions in Biomechanics and Robotics*, pages 299–324. Springer, 2006.
- [57] Hongkai Dai and Russ Tedrake. Planning robust walking motion on uneven terrain via convex optimization. In *Humanoid Robots (Humanoids), 2016 IEEE-RAS 16th International Conference on*, pages 579–586. IEEE, 2016.
- [58] Andreas Hofmann, Marko Popovic, and Hugh Herr. Exploiting angular momentum to enhance bipedal center-of-mass control. In *2009 IEEE International Conference on Robotics and Automation*, pages 4423–4429. IEEE, 2009.
- [59] Ambarish Goswami and Vinutha Kallem. Rate of change of angular momentum and balance maintenance of biped robots. In *IEEE International Conference on Robotics and Automation, 2004. Proceedings. ICRA'04. 2004*, volume 4, pages 3785–3790. IEEE, 2004.
- [60] Xiaobin Xiong and Aaron Ames. Sequential motion planning for bipedal somersault via flywheel slip and momentum transmission with task space control. *arXiv preprint arXiv:2008.02432*, 2020.
- [61] S. Kajita and K. Tani. Study of dynamic biped locomotion on rugged terrain-derivation and application of the linear inverted pendulum mode. In *Robotics and Automation, 1991. Proceedings., 1991 IEEE International Conference on*, pages 1405–1411 vol.2, 1991.
- [62] M. H. Raibert. Hopping in legged systems—modeling and simulation for the two-dimensional one-legged case. *IEEE Transactions on Systems, Man and Cybernetics*, 14(3):451–63, June 1984.
- [63] J. Pratt, J. Carff, S. Drakunov, and A. Goswami. Capture Point: A Step toward Humanoid Push Recovery. *2006 6th IEEE-RAS International Conference on Humanoid Robots*, 2006.
- [64] Xingye Da, Omar Harib, Ross Hartley, Brent Griffin, and Jessy W Grizzle. From 2D design of underactuated bipedal gaits to 3D implementation: Walking with speed tracking. *IEEE Access*, 4:3469–3478, 2016.
- [65] Majid Khadiv, Alexander Herzog, S Ali A Moosavian, and Ludovic Righetti. Walking control based on step timing adaptation. *IEEE Transactions on Robotics*, 36(3):629–643, 2020.
- [66] Carlos Gonzalez, Victor Barasuol, Marco Frigerio, Roy Featherstone, Darwin G Caldwell, and Claudio Semini. Line walking and balancing for legged robots with point feet. In *2020 IEEE/RSJ International Conference on Intelligent Robots and Systems (IROS)*, pages 3649–3656. IEEE, 2020.
- [67] Eric R Westervelt, Christine Chevallereau, Jun Ho Choi, Benjamin Morris, and Jessy W Grizzle. Feedback control of dynamic bipedal robot locomotion. CRC press, 2007.
- [68] Matthew J Powell, Ayonga Hereid, and Aaron D Ames. Speed regulation in 3d robotic walking through motion transitions between human-inspired partial hybrid zero dynamics. In *2013 IEEE international conference on robotics and automation*, pages 4803–4810. IEEE, 2013.
- [69] Jessy W Grizzle and Christine Chevallereau. Virtual constraints and hybrid zero dynamics for realizing underactuated bipedal locomotion. In Bruno Siciliano and Oussama Khatib, editors, *Springer handbook of robotics*. Springer, 2016.
- [70] Hamid Sadeghian, Christian Ott, Gianluca Garofalo, and Gordon Cheng. Passivity-based control of underactuated biped robots within hybrid zero dynamics approach. In *2017 IEEE International Conference on Robotics and Automation (ICRA)*, pages 4096–4101. IEEE, 2017.

- [71] B. Morris and J. W. Grizzle. Hybrid invariant manifolds in systems with impulse effects with application to periodic locomotion in bipedal robots. *IEEE Transactions on Automatic Control*, 54(8):1751–1764, August 2009.
- [72] C. Chevallereau, J. W. Grizzle, and C. L. Shih. Asymptotically stable walking of a five-link underactuated 3D bipedal robot. *IEEE Transactions on Robotics*, 25(1):37–50, February 2009.
- [73] A. Ames, K. Galloway, J. W. Grizzle, and K. Sreenath. Rapidly exponentially stabilizing control Lyapunov functions and hybrid zero dynamics. *IEEE Transactions on Automatic Control*, 59(4):876–891, 2014.
- [74] William Yang and Michael Posa. Impact invariant control with applications to bipedal locomotion. *arXiv preprint arXiv:2103.06907*, 2021.
- [75] Giuseppe Viola. Control of underactuated mechanical systems via passivity-based and geometric techniques. *..*, 2008.
- [76] Eric R Westervelt, Jessy W Grizzle, and C Canudas De Wit. Switching and pi control of walking motions of planar biped walkers. *IEEE Transactions on automatic control*, 48(2):308–312, 2003.
- [77] Shishir Kolathaya and Aaron D Ames. Input-to-state safety with control barrier functions. *IEEE control systems letters*, 3(1):108–113, 2018.
- [78] Sushant Veer, Ioannis Poulakakis, et al. Input-to-state stability of periodic orbits of systems with impulse effects via poincaré analysis. *IEEE Transactions on Automatic Control*, 64(11):4583–4598, 2019.
- [79] Y. Gong, R. Hartley, X. Da, A. Hereid, O. Harib, J. Huang, and J. Grizzle. Feedback control of a cassie bipedal robot: Walking, standing, and riding a segway. In *2019 American Control Conference (ACC)*, pages 4559–4566, 2019.
- [80] Hereid Ayonga. Fast Robot Optimization and Simulation Toolkit(FROST). <https://ayonga.github.io/frost-dev/>.
- [81] Ross Hartley, Maani Ghaffari, Ryan M Eustice, and Jessy W Grizzle. Contact-aided invariant extended kalman filtering for robot state estimation. *The International Journal of Robotics Research*, 39(4):402–430, 2020.
- [82] Ross Hartley. Invariant-EKF. <https://github.com/RossHartley/invariant-ekf>.
- [83] Sebastian Thrun. Probabilistic robotics. *Communications of the ACM*, 45(3):52–57, 2002.
- [84] K. Galloway, K. Sreenath, A. D. Ames, and J. W. Grizzle. Torque saturation in bipedal robotic walking through control lyapunov function-based quadratic programs. *IEEE Access*, 3:323–332, 2015.
- [85] E. R. Westervelt, G. Buche, and J. W. Grizzle. Experimental validation of a framework for the design of controllers that induce stable walking in planar bipeds. *International Journal of Robotics Research*, 24(6):559–582, June 2004.
- [86] Experiment Video Compilation. <https://youtu.be/o8msaembEu8>.
- [87] Michigan Robotics: Dynamic Legged Locomotion Lab Youtube Channel. <https://www.youtube.com/channel/UCMfDV8rkQqWhUwnTAYaq0tQ>. Accessed: 2021-05-09.
- [88] Christian Ott. *Cartesian impedance control of redundant and flexible-joint robots*. Springer, 2008.